Articles

Contribution from the Departments of Chemistry and of Material Science and Engineering, Massachusetts Institute of Technology, Cambridge, Massachusetts 02139

Osmium Imido Complexes: Synthesis, Reactivity, and SCF–Xα–SW Electronic Structure

Mark H. Schofield, Terence P. Kee, Jens T. Anhaus, Richard R. Schrock,* Keith H. Johnson, and William M. Davis

Received January 4, 1991

Osmium tetraoxide reacts with 3 equiv of 2,6-diisopropylphenyl isocyanate in refluxing heptane over a period of 20 h to afford red-brown crystalline trigonal planar $Os(NAr)_3$ (**1**; Ar = 2,6-C_6H_3-*i*-Pr_2) in modest (50%) yield. **1** reacts with relatively small phosphines and phosphites to afford square-planar complexes of the type *trans*-$Os(NAr)_2L_2$ (**4**; L = PMe_2Ph, PMe_3, $P(OMe)_3$) in high yield and with trimethylamine oxide to give $Os(NAr)_3O$, which in turn reacts with olefins $C_2H_2R_2$ to give metalla-imidazolidine complexes, Os[N(Ar)CHRCHRN(Ar)](NAr)(O). An X-ray study of the complex made from ethylene (**5b**; $P\bar{1}$, a = 9.607 (2) Å, b = 22.294 (6) Å, c = 8.997 (2) Å, α = 100.08 (2)°, β = 112.44 (2)°, γ = 90.85 (2)°, V = 1746.6 (8) Å^3, Z = 2, ρ(calcd) = 1.977 g cm^{-3}, R_1 = 0.034, R_2 = 0.047) showed it to be a pseudotetrahedral complex in which each nitrogen atom in the ring is trigonal planar. *trans*-$Os(NAr)_2(PMe_2Ph)_2$ (**4b**) reacts with Me_3NO to give $Os(NAr)_2O_2$, with methyl or ethyl iodide to give complexes of the type $Os(NAr)_2(R)I(PMe_2Ph)$, and with iodine to give $Os(NAr)_2(PMe_2Ph)I_2$ (**7**). An X-ray structure of **7** ($P2_1/n$, a = 15.2139 (9) Å, b = 14.0999 (9) Å, c = 18.158 (1) Å, β = 106.795 (4)°, V = 3729.0 (8) Å^3, Z = 4, ρ(calcd) = 1.354 g cm^{-3}, R_1 = 0.051, R_2 = 0.057) showed it to be a trigonal bipyramid with two imido ligands and one iodide in the equatorial plane. **7** reacts with KS_2CNEt_2 to give $Os(NAr)_2(S_2CNEt_2)_2$, with 2 equiv of AgOAc to give $Os(NAr)_2(OAc)_2(PMe_2Ph)$ (**12**), and with 2 equiv of MeMgCl to give $Os(NAr)_2Me_2(PMe_2Ph)$. From **12** can be prepared $Os(NAr)_2(S$-*t*-$Bu)_2$ and $Os(NAr)_2R_2$ (R = CH_2-*t*-Bu, CH_2SiMe_3). An SCF–Xα–SW analysis of $Os(NH)_3$ in D_{3h} symmetry agrees with a qualitative MO description. The HOMO ($3a_1'$) is essentially an osmium-centered weakly σ-antibonding orbital and the LUMO (2e") a low-lying π-antibonding level. The occupied $1a_2'$ orbital, which is largely nitrogen-centered (76% vs 3% osmium), prevents the species from being a true 20-electron complex. An SCF–Xα–SW analysis of $Os(NH)_2(PH_3)_2$ in C_{2h} symmetry also confirmed the qualitative MO description. The two highest occupied MO's are osmium-based ($3b_g$ (d_{xz}) and $7a_g$ (d_{z^2})) with the $7a_g$ approximately 1 eV higher in energy. The LUMO is an in-plane π* orbital ($8a_g$). An occupied nonbonding level ($6b_u$) localized almost entirely at nitrogen and phosphorus prevents this species from being a true 20-electron complex.

Introduction

A variety of interesting transition-metal complexes containing one or more organoimido ligands have been reported in the past couple of years.[1] Organoimido ligands are compatible with a variety of transition metals in many oxidation states, especially earlier metals in high oxidation states, and imido complexes are generally thought to be more stable toward bimolecular decomposition reactions than analogous oxo complexes.[2] The structures of most imido complexes fall within one of three classes, terminal linear (A), terminal bent (B), and bridging (C). Ligands of type

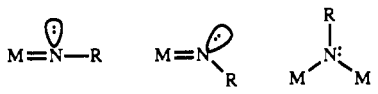

A B C

A and C usually are assumed to form another π bond to the metal to some extent by using the imido ligand's lone pair. Therefore, the imido ligand of type A can be considered isoelectronic with an alkylidyne or carbyne (M≡CR) ligand.

The (2,6-diisopropylphenyl)imido ligand (NAr) is an especially interesting one, since it is relatively bulky and therefore less prone to bridge between metals than (e.g.) a *tert*-butylimido ligand. Efforts in our laboratories over the past several years have been directed toward using the NAr ligand to stabilize molybdenum,[1t] tungsten,[1u,v] and rhenium[1r,w,x] in high oxidation states. Recently we have undertaken an investigation of the potential of this ligand to stabilize relatively high oxidation states of metals in group 8. In a preliminary communication,[1s] we reported the synthesis of two planar imido complexes, $Os(NAr)_3$ (**1**) and *trans*-$Os(NAr)_2(PMe_2Ph)_2$ (**2**). A common feature of **1** and **2** are occupied ligand-centered nonbonding orbitals, which prevent electronic supersaturation of the metal center. In this paper we report these and other recent developments in the area of high oxidation state osmium imido chemistry, qualitative molecular orbital analyses supported by SCF–Sα–SW calculations,[3,4] and crystal structures

* To whom correspondence should be addressed at the Department of Chemistry.

(1) (a) Burns, C. J.; Smith, W. H.; Huffman, J. C.; Sattelberger, A. P. *J. Am. Chem. Soc.* **1990**, *112*, 3237. (b) Chao, Y.-W.; Wexler, P. A.; Wigley, D. E. *Inorg. Chem.* **1989**, *28*, 3860. (c) Clark, G. R.; Nielson, A. J.; Rickard, C. E. F. *J. Chem. Soc., Chem. Commun.* **1989**, 1157. (d) Cummins, C. C.; Baxter, S. M.; Wolczanski, P. T. *J. Am. Chem. Soc.* **1988**, *110*, 8731. (e) Danapoulos, A. A.; Wilkinson, G.; Hussain, B.; Hursthouse, M. B. *J. Chem. Soc., Chem. Commun.* **1989**, 896. (f) Danopoulos, A. A.; Wilkinson, G. *Polyhedron* **1990**, *9*, 1009. (g) de With, J.; Horton, A. D.; Orpen, A. G. *Organometallics* **1990**, *9*, 2207. (h) Ge, Y.-W.; Sharp, P. R. *J. Am. Chem. Soc.* **1990**, *112*, 3667. (i) Glueck, D. S.; Hollander, F. J.; Bergman, R. G. *J. Am. Chem. Soc.* **1989**, *111*, 2719. (j) Harlan, E. W.; Holm, R. H. *J. Am. Chem. Soc.* **1990**, *112*, 186. (k) Herrmann, W. A.; Weichselbaumer, G.; Paciello, R. A.; Fischer, R. A.; Herdtweck, E.; Okuda, J.; Marz, D. W. *Organometallics* **1990**, *9*, 489. (l) Maatta, E. A.; Kim, C. *Inorg. Chem.* **1989**, 428, 624. (m) Meijboom, N.; Schaverien, C. J.; Orpen, A. G. *Organometallics* **1990**, *9*, 774. (n) Profilet, R. D.; Zambrano, C. H.; Fanwick, P. E.; Nash, J. J.; Rothwell, I. P. *Inorg. Chem.* **1990**, *29*, 4362. (o) Su, F. M.; Bryan, J. C.; Jang, S.; Mayer, J. M. *Polyhedron* **1989**, *8*, 1261. (p) Walsh, P. J.; Hollander, F. J.; Bergman, R. G. *J. Am. Chem. Soc.* **1988**, *110*, 8729. (q) Marshman, R. W.; Shapley, P. A. *J. Am. Chem. Soc.* **1990**, *112*, 8369. (r) Horton, A. D.; Schrock, R. R. *Polyhedron* **1988**, *7*, 1841. (s) Anhaus, J. T.; Kee, T. P.; Schofield, M.; Schrock, R. R. *J. Am. Chem. Soc.* **1990**, *112*, 1642. (t) Schrock, R. R.; Murdzek, J. S.; Bazan, G. C.; Robbins, J.; DiMare, M.; O'Regan, M. *J. Am. Chem. Soc.* **1990**, *112*, 3875. (u) Schrock, R. R.; DePue, R. T.; Feldman, J.; Yap, K. B.; Yang, D. C.; Davis, W. M.; Park, L. Y.; DiMare, M.; Schofield, M.; Anhaus, J.; Walborsky, E.; Evitt, E.; Krüger, C.; Betz, P. *Organometallics* **1990**, *9*, 2262. (v) Williams, D. S.; Schofield, M. H.; Anhaus, J. T.; Crowe, W. E.; Schrock, R. R. *J. Am. Chem. Soc.* **1990**, *112*, 6728. (w) Weinstock, I. A.; Schrock, R. R.; Davis, W. M. *J. Am. Chem. Soc.* **1990**, *112*, 135. (x) Weinstock, I. A.; Schrock, R. R.; Williams, D. S.; Crowe, W. E. *Organometallics* **1991**, *9*, 1. (y) Danopoulous, A. A.; Wilkinson, G.; Hussain-Bates, B.; Hursthouse, M. B. *J. Chem. Soc., Dalton Trans.* **1991**, 269. (z) Glueck, D. S.; Wu, J.; Hollander, F. J.; Bergman, R. C. *J. Am. Chem. Soc.* **1991**, *113*, 2041.

(2) (a) Nugent, W. A.; Haymore, B. L. *Coord. Chem. Rev.* **1980**, *31*, 123. (b) Nugent, W. A.; Mayer, J. M. *Metal-Ligand Multiple Bonds*; Wiley-Interscience: New York, 1988.

0020-1669/91/1330-3595$02.50/0

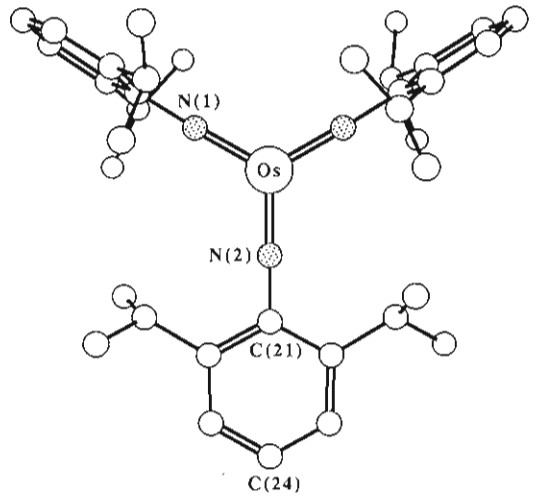

Figure 1. Drawing of the structure of $Os(N\text{-}2,6\text{-}C_6H_3\text{-}i\text{-}Pr_2)_3$ (**1**).

Table I. Selected Bond Distances (Å) and Angels (deg) in $Os(NAr)_3$ (**1**) and *trans*-$Os(NAr)_2(PMe_2Ph)_2$ (**4b**)

		1	
Os–N(1)	1.736 (5)	N(1)–Os–N(1)′	119.8 (3)
Os–N(2)	1.738 (7)	N(1)–Os–N(2)	120.1 (2)
N(1)–C(11)	1.383 (7)	Os–N(1)–C(11)	178.0 (5)
N(2)–C(21)	1.36 (1)	Os–N(2)–C(21)	180 (3)
		4b	
Os–N(1)	1.790 (6)	N(1)–Os–P(1)	89.1 (2)
Os–P(1)	2.374 (2)	Os–N(1)–C(11)	177.9 (5)
N(1)–C(11)	1.825 (9)	Os–P(1)–C(41)	116.6 (3)

of two new Os(VI) complexes, a five-coordinate bis(imido) diiodide complex and an oxo imido metallaimidazolidine complex.

Results

Synthesis and Characterization of $Os(NAr)_3$ (1). Osmium tetroxide reacts with 3 equiv of 2,6-diisopropylphenyl isocyanate in refluxing heptane over a period of 20 h to afford red-brown crystalline $Os(NAr)_3$ (**1**) in modest (50%) yield (eq 1). An X-ray

$$OsO_4 + 3ArNCO \xrightarrow[\text{reflux, 20 h}]{\text{heptane}} Os(NAr)_3 \qquad (1)$$

study[1a] showed **1** to be a trigonal-planar complex (Figure 1) in which a crystallographic 2-fold axis passes through Os, N(2), C(21), and C(24). Relevant bond angles and distances are listed in Table I. Two of the phenyl rings are oriented roughly perpendicular to the OsN_3 plane (dihedral angle 81.62°), while the third lies in the OsN_3 plane (dihedral angle 1.90°). Os–N distances are relatively short, and Os–N–C angles are close to 180°. Since the proton NMR spectrum of **1** (which shows only a single type of imido ligand) is unchanged in a sample at −90 °C, the phenyl rings either freely rotate about the $N\text{–}C_{ipso}$ bond or in solution the planes of the phenyl rings are all perpendicular to the OsN_3 plane.

Scheme I summarizes the reactivity of **1**. The NMR spectrum of **2** shows it to be a symmetric species. The structure shown is based on the analogy with known d^2 octahedral dioxo complexes (see Discussion); a symmetric structure containing cis imido ligands in which rotation about the $N\text{–}C_{ipso}$ bond is facile is an alternative that cannot be discounted. **1** does not react with Lewis bases such as triphenylphosphine, triphenylarsine, quinuclidine, pyridine, or ethyldimethylamine. However, **1** does react with less sterically demanding phosphines and phosphites to afford complexes of the type *trans*-$Os(NAr)_2L_2$ in high yield. (Phosphinimines were observed products by proton NMR.) There are several examples in the literature of phosphine-induced reductive deaminations of transition-metal imido complexes.[1j]

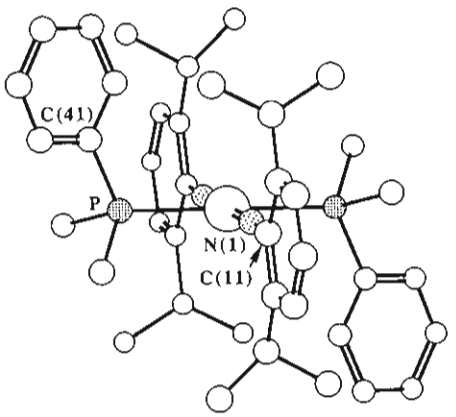

Figure 2. Drawing of the structure of *trans*-$Os(N\text{-}2,6\text{-}C_6H_3\text{-}i\text{-}Pr_2)_2(PMe_2Ph)_2$ (**4b**).

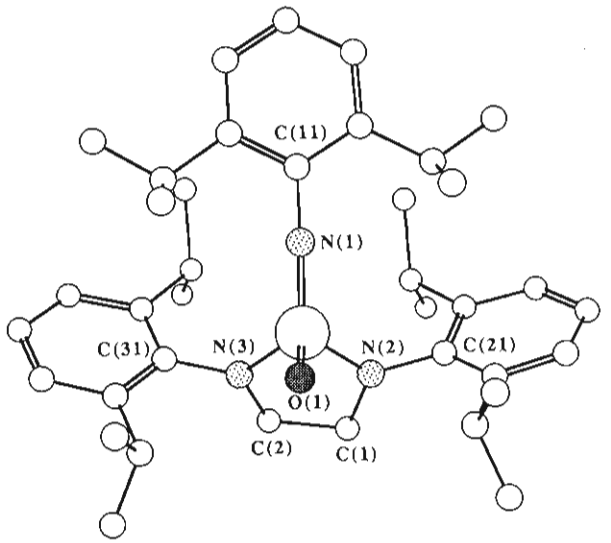

Figure 3. Drawing of the structure of *trans*-$Os[N(Ar)CH_2CH_2N(Ar)](NAr)(O)$ (**5a**).

Scheme I. Reactions of $Os(NAr)_3$ (**1**)

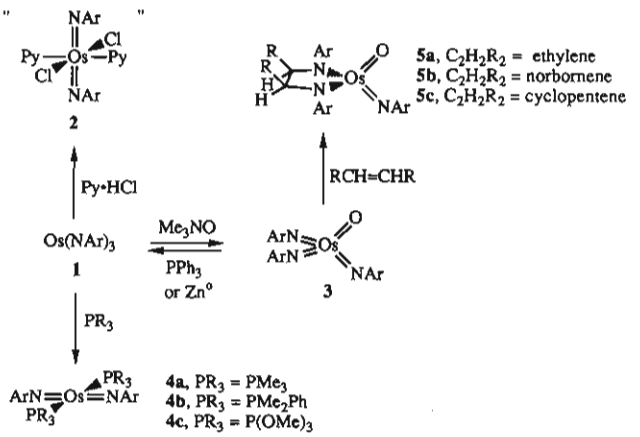

An X-ray study showed **4b** to be square planar with an inversion center (Figure 2, Table I) and virtually linear imido ligands (Os–N–C = 177.9 (5)°). The Os–N bond lengths in **4b** are slightly longer than they are in **1**, perhaps largely because of the higher coordination number and lower oxidation state of the metal.

One of the original goals of this research was to prepare $Os(NAr)_3(O)$. We hoped to show that it did not (for steric reasons) react with olefins to give metallaimidazolidine complexes, as other $Os(NR)_3(O)$ complexes have been shown to do.[5] However, **3**

(3) Johnson, K. H. *Adv. Quantum Chem.* **1972**, *7*, 143.
(4) Case, D. A. *Annu. Rev. Phys. Chem.* **1982**, *33*, 151.
(5) Chong, A. O.; Oshima, K.; Sharpless, K. B. *J. Am. Chem. Soc.* **1977**, *99*, 3420.

Table II. Selected Bond Distances (Å) and Angles (deg) in $Os[N(Ar)CH_2CH_2N(Ar)](NAr)(O)$ (**5a**)

Os–N(1)	1.71 (1)	N(2)–C(1)	1.48 (1)
Os–O(1)	1.729 (8)	N(3)–C(2)	1.47 (1)
Os–N(2)	1.896 (9)	C(1)–C(2)	1.49 (2)
Os–N(3)	1.922 (8)		
N(1)–Os–O(1)	115.2 (4)	Os–N(2)–C(21)	126.0 (6)
N(1)–Os–N(2)	117.0 (4)	Os–N(1)–C(11)	177.5 (8)
N(1)–Os–N(3)	116.2 (4)	Os–N(3)–C(31)	124.5 (7)
O(1)–Os–N(2)	111.2 (4)	N(3)–C(2)–C(1)	109.2 (8)
N(2)–Os–N(3)	80.3 (4)	C(21)–N(2)–C(1)	114.7 (9)
Os–N(2)–C(1)	119.1 (7)	C(31)–N(3)–C(2)	115.6 (8)
Os–N(3)–C(2)	119.7 (7)	N(2)–C(1)–C(2)	108.4 (8)

Scheme II. Reactions of *trans*-$Os(NAr)_2(PMe_2Ph)_2$ (**4b**)

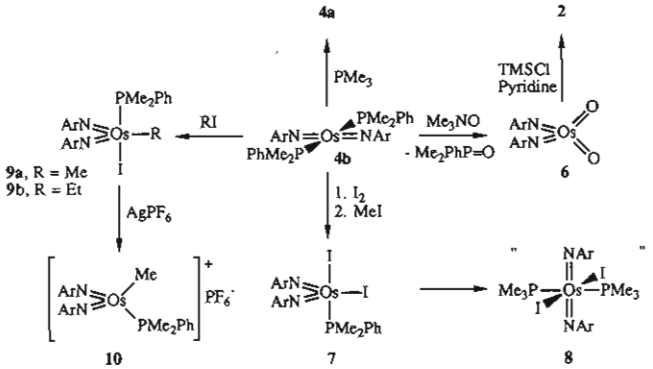

reacts cleanly with ethylene, norbornene, and cyclopentene to afford, in each case, a single product with the general formula $Os[N(Ar)CHRCHRN(Ar)](NAr)(O)$ (**5a–c**). An X-ray study of **5a** revealed that the metallaimidazolidine complex has pseudotetrahedral geometry (Figure 3, Table II) in which the average bond angle at osmium is ~109°. The terminal Os–O and Os–N distances are not unusual, and the Os–N(1)–C(11) angle is again close to being linear. The trigonal-planar geometry about each nitrogen atom in the metallaimidazolidine ring and the quite short Os–N distance could be taken as evidence of a significant degree of π bonding between Os and N. Tetrahedral d^2 complexes containing several multiply bonded ligands are relatively uncommon.[6,8]

Reactivity of *trans*-$Os(NAr)_2(PMe_2Ph)_2$ (4b). A summary of the reactivity of **4b** is shown in Scheme II. It reacts with excess PMe_3 (7 equiv) in C_6D_6 rapidly at room temperature to afford $Os(NAr)_2(PMe_3)_2$ (**4a**) quantitatively (by ^1H NMR). There is no evidence (by NMR) for the formation of $Os(NAr)_2(PMe_2Ph)(PMe_3)$. In contrast, **4b** does not react with PPh_3 (2 equiv) after 8 h at 70 °C in C_6D_6. However, **4b** *will* react with $P(OMe)_3$ (7 equiv) smoothly at 25 °C to afford an equilibrium mixture of $Os(NAr)_2(PMe_2Ph)[P(OMe)_3]$ (**4d**) and $Os(NAr)_2[P(OMe)_3]_2$ (**4c**) along with **4b** (eqs 2 and 3). The equilibrium

$$Os(NAr)_2(PMe_2Ph)_2 + P(OMe)_3 \rightleftharpoons Os(NAr)_2(PMe_2Ph)[P(OMe)_3] + PMe_2Ph \quad (2)$$

$$Os(NAr)_2(PMe_2Ph)[P(OMe)_3] + P(OMe)_3 \rightleftharpoons Os(NAr)_2[P(OMe)_3]_2 + PMe_2Ph \quad (3)$$

constants for these processes (by ^1H NMR) are $K_2 = 0.08$ and $K_3 = 0.012$ (at 302 K). On this basis the trend for phosphorus base affinity for "$Os(NAr)_2$" appears to be $PMe_3 > PMe_2Ph > P(OMe)_3 > PPh_3$. Free PMe_2Ph does not exchange with coordinated PMe_2Ph in **4b** in C_6D_6 on the NMR time scale at 25 °C.

4b can be oxidized with Me_3NO to afford $Os(NAr)_2O_2$ (**6**) in 45% yield, some **1**, and $Me_2PhP{=}O$. A mechanism for formation of **1** might consist of disproportionation of intermediate "$Os(NAr)_2O$". The reaction between **6**, (TMS)Cl, and pyridine yields $Os(NAr)_2Cl_2(py)_2$ (**2**). **4b** also is oxidized by alkyl iodides to afford five-coordinate complexes of the type $Os(NAr)_2(R)I(PMe_2Ph)$ (**9a**, R = Me; **9b**, R = Et). **9a** can be converted to a four-coordinate cationic, presumably tetrahedral $[Os(NAr)_2(R)(PMe_2Ph)]PF_6$ by treatment with $AgPF_6$. Addition of iodine to **4b** followed by 1 equiv of MeI (to scavenge excess phosphine) yields five-coordinate $Os(NAr)_2I_2(PMe_2Ph)$ (**7**) in high yield. The PMe_2Ph ligand in **7** can be replaced readily by PMe_3 to yield $Os(NAr)_2I_2(PMe_3)_2$ (**8**) quantitatively (by NMR); the structure shown for **8** is a likely but as yet unconfirmed possibility (see Discussion).

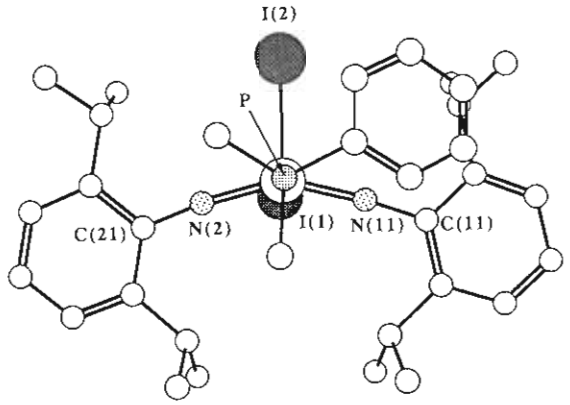

Figure 4. Drawing of the structure of $Os(NAr)_2I_2(PMe_2Ph)$ (**7**).

Table III. Selected Bond Distances (Å) and Angles (deg) in $Os(NAr)_2I_2(PMe_2Ph)$ (**7**)

Os–N(11)	1.770 (6)	Os–I(1)	2.8229 (8)
Os–N(2)	1.775 (6)	Os–I(2)	2.6261 (9)
Os–P	2.340 (2)		
N(11)–Os–N(2)	151.2 (3)	N(2)–Os–I(1)	87.9 (2)
N(11)–Os–P	90.0 (2)	P–Os–I(2)	91.32 (7)
N(11)–Os–I(2)	104.2 (2)	P–Os–I(1)	174.41 (6)
N(11)–Os–I(1)	88.0 (2)	Os–N(2)–C(21)	171.2 (5)
N(2)–Os–P	91.3 (2)	I(2)–Os–I(1)	94.24 (3)
N(2)–Os–I(2)	104.5 (2)	Os–N(11)–C(11)	168.2 (5)

Table IV. Crystallographic Data for $Os(NArCH_2CH_2NAr)(NAr)O$ (**5a**) and $Os(NAr)_2I_2(PMe_2Ph)$ (**7**)

	5a	**7**
emp formula	$OsC_{40}H_{56}I_2N_2P$	$OsC_{38}H_{55}N_3O$
fw	1039.88	760.07
cryst system	triclinic	monoclinic
a, Å	9.607 (2)	15.2139 (9)
b, Å	22.294 (6)	14.0999 (9)
c, Å	8.997 (2)	18.158 (1)
α, deg	100.08 (2)	90
β, deg	112.44 (2)	106.795 (4)
γ, deg	90.85 (2)	90
V, Å^3	1746.6 (8)	3729.0 (8)
space group	$P\bar{1}$	$P2_1/n$
Z	2	4
ρ(calcd), g/cm^3	1.977	1.354
μ, cm^{-1}	54.80	34.51
final R_1, R_2	0.034, 0.047	0.051, 0.057
max peak in final diff map, e/Å^3	1.25	1.56
min peak in final diff map, e/Å^3	0.62	−1.51

An X-ray study of **7** (Figure 4, Tables III and IV) showed it to be a trigonal bipyramid with two imido ligands and one iodide in the equatorial plane. Both imido ligands are close to being linear (Os–N(11)–C(11) = 168.2 (5)°; Os–N(2)–C(21) = 171.2 (5)°). The trans influence of the PMe_2Ph ligand is manifested by a longer Os–I(1) distance of 2.8229 (8) Å compared to Os–I(2) of 2.6261 (9) Å. An interesting feature is that the Ar rings lie in the equatorial plane and that the N(11)–Os–N(2) angle (151.2 (3)°) is significantly larger than those found for the isostructural d^0 complexes $Re(N\text{-}t\text{-}Bu)_2X_2Y$ (X = Y = Cl; X = Cl, Y = Ph)

(6) Griffith, W. P.; McManus, N. T.; Skapski, A. C.; Nielson, A. J. *Inorg. Chim. Acta* **1985**, *103*, L5.
(7) Danapoulos, A. A.; Longley, C. J.; Wilkinson, G.; Hussain, B.; Hursthouse, M. B. *Polyhedron* **1989**, *8*, 2657.
(8) Laine, R. M.; Moriarty, R. E.; Bau, R. *J. Am. Chem. Soc.* **1972**, *94*, 1402.

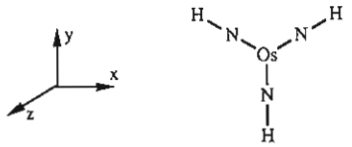

Figure 5. Orientation and coordinate system for $Os(NH)_3$ model in D_{3h} symmetry. All atoms lie in the xy plane.

Scheme III. Reactions of *trans*-$Os(NAr)_2I_2(PMe_2Ph)$ (7)

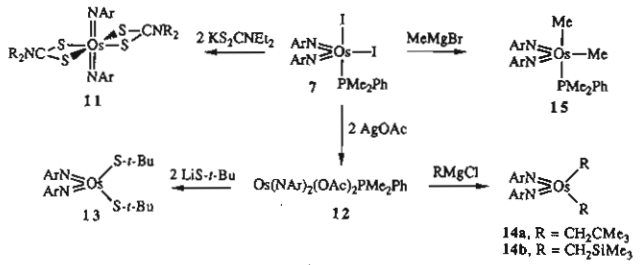

studied by Wilkinson and co-workers (ca. 110°).[7] At this stage it is not known whether this circumstance can be ascribed to sterics (the isopropyl substituents in the imido ligands discourage the plane of each aryl ring from orienting perpendicular to the equatorial plane) or whether electronic factors (see Discussion) also play a major role.

Reactivity of $Os(NAr)_2I_2(PMe_2Ph)$ (7). Some reactions of **7** are summarized in Scheme III. Both iodides and the phosphine can be displaced by 2 equiv of potassium diethyldithiocarbamate to afford *trans*-$Os(NAr)(S_2CNEt_2)_2$ in 71% yield. **7** also reacts with 2 equiv of AgOAc to afford $Os(NAr)_2(OAc)_2(PMe_2Ph)$ (**12**). **12** is stable to moist air in the solid state for at least 1 week at ambient temperature but readily coordinates a second molecule of PMe_2Ph or 2 equiv of PMe_3 to form complexes of the type $Os(NAr)_2(OAc)_2L_2$ quantitatively (by ^1H NMR). The acetates and imido ligands in **12** remain equivalent down to −80 °C. **12** reacts readily with LiO-*t*-Bu, $LiOCMe(CF_3)_2$, or $LiOC_6H_3Me_2$, but the only product that could be identified was **4b** in ~50% yield. However, **12** *does* react with LiS-*t*-Bu in toluene to afford red, crystalline $Os(NAr)_2(S\text{-}t\text{-}Bu)_2$ (**13**) in 70% yield. We propose that **12** is pseudotetrahedral by analogy with recently characterized d^2 bis(imido) complexes of tungsten(IV)[1v] and rhenium(V).[1x] **12** also reacts readily with RCH_2MgCl in diethyl ether to afford complexes of the type $Os(NAr)_2(CH_2R)_2$ (**14a**, R = *t*-Bu; **14b**, R = $SiMe_3$) as orange-red crystals in moderate yield (**14a**, 53%; **14b**, 67%). The dominant byproduct in each case is **4b**, which presumably forms by a competitive reductive process.

We thought that **7** might be a suitable intermediate for synthesizing alkyl complexes of osmium(VI). Unfortunately, it appears to be reduced relatively readily; i.e., **7** reacts with PhMgCl, (cyclopentyl)MgCl, *t*-$BuCH_2MgCl$, and $(t\text{-}BuCH_2)_2Zn$ in diethyl ether between 0 and −40 °C to form $Os(NAr)_2(PMe_2Ph)_2$ as the only characterizable product in up to 50% isolated yield. However, **7** could be alkylated cleanly by 2 equiv of MeMgBr in ether at 25 °C to afford blue, crystalline $Os(NAr)_2Me_2(PMe_2Ph)$ (**15**) in 82% yield. NMR studies of **15** suggest that the structure of **15** is analogous to that of **7**.

Molecular Orbital Description and SCF–Xα–SW Analysis of $Os(NH)_3$ in D_{3h} Symmetry. In $Os(NH)_3$ (Figure 5) the nitrogen σ orbitals transform as $A_1' + E'$ and interact with the metal s, p_x, p_y, and d_{z^2} (which becomes weakly antibonding) to form three σ-type molecular orbitals. The nitrogen p_z orbitals transform as $A_2'' + E''$ and interact with the osmium p_z, d_{xz}, and d_{yz} atomic orbitals, forming the $\pi_\parallel$ orbitals (parallel to the z axis). The nitrogen in-plane p orbitals transform as $A_2' + E'$. The d_{xy} and $d_{x^2-y^2}$ orbitals constitute the e′ set and interact with the E′ combination to form two $\pi_\perp$ orbitals (perpendicular to the z axis). There are no osmium orbitals of A_2' symmetry, however, rendering the nitrogen a_2' combination nonbonding. In $Os(NH)_3$, if the imido ligand is counted as a dianion, osmium can be considered to be in the +6 oxidation state (d^2). Addition of the 20 electrons total contributed by the imido ligands and Os leads to 2 electrons

Table V. Xα Valence Molecular Orbitals for $Os(NH)_3$ in D_{3h}[a]

level	energy, eV	occup[c]	charge distribution, % Os	N	H	Os basis functions[d]
$2a_2''$	−1.132	0	1	7	0	p_z(75), f(25)
$4a_1'$	−1.360	0	6	3	0	s(1), d_{z^2}(88), f(11)
$4e'$	−2.725	0	45	35	6	p_x,p_y(5), $d_{x^2-y^2}$,d_{xy}(95)
$2e''$	−4.753	0	43	39	1	d_{xz},d_{yz}(99), f(1)
$3a_1'$	−7.300	2	69	3	1	s(14), d_{z^2}(86)
$1a_2'$	−7.816	2	3	76	1	f(100)
$1a_2''$	−8.195	2	4	67	1	p_z(72), f(28)
$3e'$	−9.221	4	15	58	3	p_x,p_y(34), $d_{x^2-y^2}$(62), f(3)
$1e''$	−10.554	4	47	36	0	d_{xz},d_{yz}(99), f(1)
$2e'$	−17.350	4	34	53	13	p_x,p_y(16), $d_{x^2-y^2}$,d_{xy}(81), f(3)
$2a_1'$	−18.458	2	26	57	17	s(41), d_{z^2}(46), f(13)
$1e'$	−24.691	4	5	68	27	p(34), d(61), f(6)
$1a_1'$	−25.181	2	8	69	23	s(46), d(35), f(19)

[a] Coordinate system is shown in Figure 5. Levels above $3a_1'$ are virtual (unoccupied) levels. [b] % of total charge density (not normalized) assigned for each atom. [c] Occupancy in electrons. [d] Breakdown of spherical harmonics for osmium basis functions. For example, of the 69% of the total charge density calculated at osmium in level $3a_1'$, 14% of this is s character and 86% is d_{z^2} character.

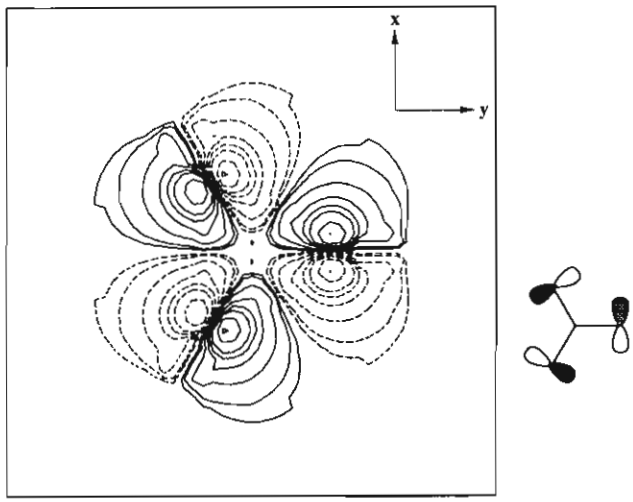

Figure 6. Wave function contour map of orbital $1a_2'$ in xy plane. Solid and dashed lines correspond to positive and negative signs for the wave function. Contours are drawn for charge densities ±0.4, ±0.2, ±0.15, ±0.1, ±0.075, ±0.5, ±0.025, ±0.01, and ±0.005 $(e/bohr^2)^{1/2}$. (Charge densities are the same for all subsequent contour maps.)

in the nitrogen-centered nonbonding orbital (a_2'). Therefore, in this orbital description, $Os(NAr)_3$ is a coordinatively saturated complex with only 18 valence electrons associated with the metal center.

This orbital description is closely related to that derived for $W(CO)(PhC{\equiv}CPh)_3$[8] and $Zr(BH_4)_4$.[9] In each case, the lack of sufficient metal-centered orbitals of the correct symmetry prevents electronic supersaturation of the metal. Chu and Hoffmann[10] have suggested that one possible role for such nonbonding (or peripheral) orbitals is the storage and retrieval of excess electrons in low-energy states and therefore access to a number of potential products along the reaction coordinate.

An analysis of the bonding in $Os(NH)_3$ by SCF–Xα–SW is in good agreement with the qualitative MO description. Table V lists the calculated ground-state two-electron energies, occupation, charge distribution, and partial breakdown of the valence molecular orbitals for $Os(NH)_3$ in D_{3h} symmetry. Wave function contour maps[11] of the HOMO, LUMO, and nonbonding (a_2') orbital are shown in Figures 6–8. In this analysis the structure

(9) Davison, A.; Wreford, S. S. *Inorg. Chem.* **1975**, *14*, 703.
(10) Chu, S.-Y.; Hoffmann, R. *J. Phys. Chem.* **1982**, *86*, 1289.
(11) Contour maps were generated by using program PIXM written by Mr. Craig Counterman, whose assistance in the program's operation is gratefully ackdnowledged.

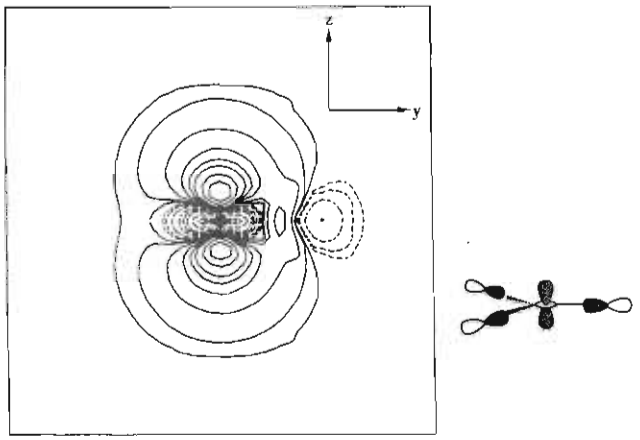

Figure 7. Wave function contour map of orbital $3a_1'$ (HOMO) in the yz plane.

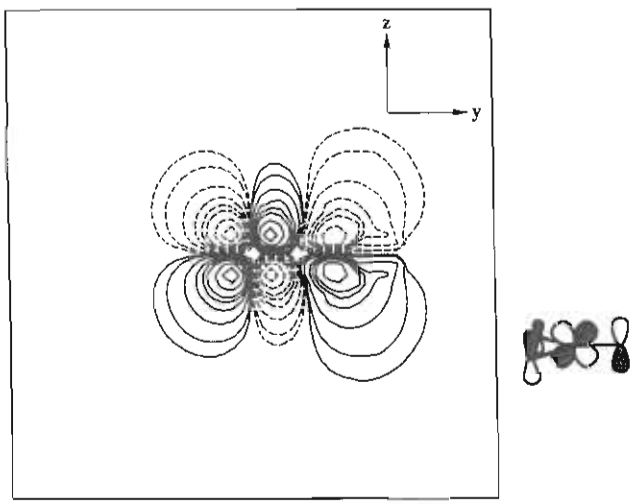

Figure 8. Wave function contour map of orbital $2e''$ (LUMO) in the yz plane.

was assumed to have idealized geometry in which all Os–N–H angles are 180°, N–Os–N = 120°, Os–N = 1.74 Å (from the X-ray structure), and N–H = 1.0 Å.[12]

The out-of-plane π orbitals ($2e''$) are approximately 1.3 eV more stable than the in-plane π orbitals ($3e'$). This is easily understood in terms of ligand-field splitting. The nitrogen σ orbitals interact more strongly with the e′ (d_{xy}, $d_{x^2-y^2}$) orbitals than the e″ (d_{xz}, d_{yz}) orbitals. The e′ levels are raised in energy and so interact less strongly with the nitrogen 2p orbitals for the formation of in-plane π molecular orbitals. The e″ orbitals are not perturbed to as great an extent by the σ interactions and can interact more strongly with the nitrogen p orbitals, forming the more stable out-of-plane π molecular orbitals. The next π orbital ($1a_2''$) is only ~0.4 eV more stable than the $1a_2'$ orbital (Figure 6) due largely to the great energetic disparity of the osmium $6p_z$ and nitrogen $2p_z$ atomic orbitals. The $1a_2''$ level is bonding; however, it is largely nitrogen-centered, as shown by the greater density of charge found on nitrogen (67% vs 4% osmium). The $1a_2'$ orbital is largely nitrogen-centered (76% vs 3% osmium) because there are no s, p, or d orbitals of appropriate symmetry to interact with the A_2' combination of nitrogen p orbitals; the 3% of charge located at osmium is pure f character. As with the $1a_2''$ orbital, the great energy disparity between the nitrogen 2p and osmium 4f appears to render this interaction weak, at best. The HOMO ($3a_1'$, Figure 7), is essentially an osmium-centered (69% vs 3% nitrogen) weakly σ-antibonding orbital. The LUMO ($2e''$, Figure 8) is a low-lying π-antibonding level.

(12) Jesson, J. P.; Muetterties, E. L. *Chemist's Guide*; Marcel Dekker: New York, 1969.

(13) Note: Subsequent to this initial calculation, a more stringent criterion for convergence was applied that resulted in a reversal of the $3b_g$ and $6b_u$ levels. Since this calculation only crudely models complex **46** and since the frontier orbital description is not otherwise dramatically affected, this does not dispute any of the essential features that arose from either the qualitative analysis or the initial calculation.

Table VI. Xα Valence Molecular Orbitals for $Os(NH)_2(PH_3)_2$ in C_{2h}[a]

level	energy, eV	occup[c]	charge distribution, % Os	N	P	Os basis functions[d]
$9a_g$	−3.964	0	42	13	21	s(6), $d_{z^2-y^2}$(94)
$4b_g$	−5.732	0	57	32	0	d_{yz}(100)
$8a_g$	−5.866	0	52	35	2	d_{xy}(100)
$7a_g$	−7.271	2	71	2	6	s(6), d_{z^2}(94)
$3b_g$	−8.296	2	82	0	4	d_{xz}(100)
$6b_u$	−9.422	2	3	51	30	p(13), f(87)
$5b_u$	−10.815	2	5	29	41	p(91), f(9)
$2a_u$	−10.048	2	3	78	0	p_z(38), f(62)
$2b_g$	−11.734	2	35	50	0	d_{yz}(100)
$6a_g$	−11.758	2	32	44	5	d_{xy}(100)
$5a_g$	−12.449	2	32	1	51	s(13), $d_{x^2-y^2}$,d_{z^2}(87)
$3b_u$	−17.487	2	21	70	0	p(66), f(34)
$2a_g$	−21.583	2	33	57	0	s(16), d(84)

[a] Coordinate system is shown in Figure 9. Levels above $7a_g$ are virtual (unoccupied) levels. [b] % of total charge density (not normalized) excluding intersphere and outer-sphere regions. [c] Occupancy in electrons. [d] Breakdown of spherical harmonics for osmium basis functions. For example, of the 71% of the total charge density calculated at osmium in level $7a_g$, 6% of this is s character and 94% is d_{z^2} character.

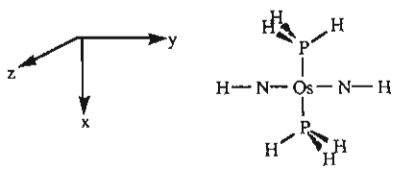

Figure 9. Orientation and coordinate system for *trans*-$Os(NH)_2(PH_3)_2$ in C_{2h} symmetry.

Molecular Orbital Description and SCF–Xα–SW Analysis of $Os(NH)_2(PH_3)_2$ in C_{2h} Symmetry. In $Os(NH)_2(PH_3)_2$ the nitrogen and phosphorus σ orbitals transform as $2A_g + 2B_u$. The metal 6s, $6p_x$, $6p_y$, and $5d_{x^2-y^2}$ orbitals are used to form the σ molecular orbitals. (The $5d_{z^2}$ orbital also interacts with the ligand σ orbitals and becomes weakly antibonding.) The nitrogen $2p_z$ orbitals transform as $B_g + B_u$, and both sets of linear combinations find a symmetry match with osmium-centered orbitals $5d_{yz}$ and $6p_z$, respectively, forming two $\pi_\parallel$ orbitals. The in-plane nitrogen orbitals (p_y) transform as $B_g + B_u$. The osmium $5d_{xy}$ orbital is of B_g symmetry and forms one $\pi_\perp$ molecular orbital; however, there are no remaining osmium-centered orbitals of B_u symmetry, as both of the osmium p_x and p_y have been energetically removed by σ-bonding interactions. Like the a_2' orbital in $Os(NH)_3$, which is ligand-centered and nonbonding, we can expect to find a nitrogen-centered orbital of B_u symmetry that is substantially nonbonding. In $Os(NH)_2(PH_3)_2$, the osmium can be considered to be in the +4 oxidation state (d^4). Of the total of 20 electrons available 2 electrons remain localized in a nitrogen-centered nonbonding orbital of B_u symmetry. Therefore, $Os(NAr)_2(PMe_2Ph)_2$ is also a coordinatively saturated complex with only 18 valence electrons associated with metal center.

Table VI presents the calculated ground-state two-electron energies, occupation, charge distribution, and partial breakdown of the relevant molecular orbitals for $Os(NH)_2(PH_3)_2$ in C_{2h} symmetry. Figure 9 shows the coordinate system for this analysis. The structure is assumed to have idealized geometry in which all of the Os–N–H angles are 180°, N–Os–N = 180°, P–Os–P = 180°, Os–H–P = 133°, Os–N = 1.74 Å, Os–P = 2.37 Å (from the X-ray structure), N–H = 1.0 Å,[14] and P–H = 1.46 Å.[14] Wave

(14) Cotton, F. A. *Chemical Applications of Group Theory*; Wiley: New York, 1971.

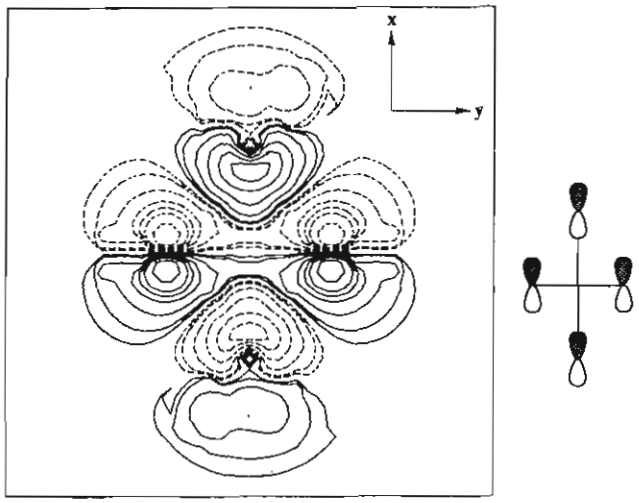

Figure 10. Wave function contour map of orbital $6b_u$ in the xy plane.

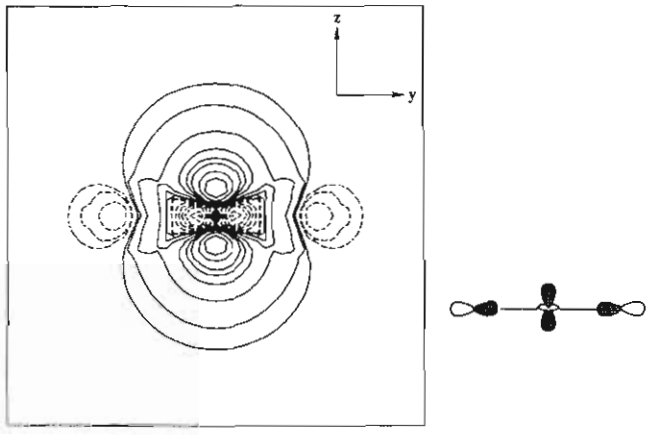

Figure 11. Wave function contour map of orbital $7a_g$ (HOMO) in the yz plane.

function contour maps of the HOMO, LUMO, and a nonbonding level are shown in Figures 10–12.

The two lowest lying π orbitals are of similar energies. At slightly lower energy is the in-plane $6a_g$ orbital. It is generated from a pure osmium $5d_{xy}$ and two nitrogen $2p_x$ orbitals. The contribution of phosphorus to this molecular orbital is quite small (5% charge density localized at phosphorus); however, it is predominantly of d character, suggesting that there is some participation of virtual d orbitals in this model. The other relatively stable π orbital is the out-of-plane $2b_g$, which consists of pure d_{yz} character at the metal. At approximately 1.7 eV higher energy is the other out-of-plane π orbital ($2a_u$), which contains osmium $6p_z$ and the in-phase combination of nitrogen $2p_z$ orbitals. As observed for the $Os(NH)_3$ $1a_2''$ level, the contribution of osmium to this molecular orbital is small because the osmium $6p_z$ orbital is energetically mismatched with the nitrogen p orbitals; it is too high in energy for reasonable overlap. Accordingly, this level is only 0.6 eV more stable than the nitrogen-centered, nonbonding $6b_u$ level (Figure 10). This nonbonding level is localized almost entirely at nitrogen and phosphorus. The fact that there is no significant contribution from osmium to the $6b_u$ level is the result of the σ interactions with the ligand set, which raise the osmium $6p_x$ orbital energy making it energetically inaccessible for π-bonding to nitrogen. The two highest occupied molecular orbitals are osmium based, $3b_g$ (d_{xz}) and $7a_g$ (d_{z^2}, Figure 11) with the $7a_g$ approximately 1 eV higher in energy. The $3b_g$ orbital does have a small (5%) contribution of predominantly phosphorus d character, which seems to implicate a weak back-bonding interaction with the phosphine ligand. The LUMO is an in-plane π^* orbital ($8a_g$, Figure 12). However, as observed with the two low-lying π-bonding orbitals, the energy gap between the in-plane and the out-of-plane π^* orbitals is quite small; the two π^* levels therefore could be considered degenerate states.[13]

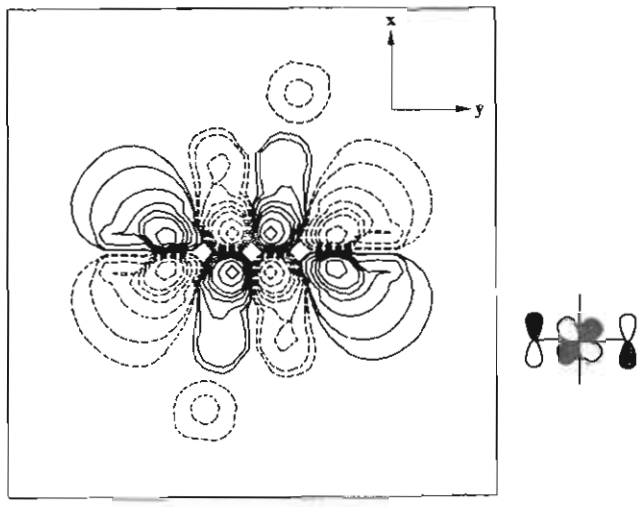

Figure 12. Wave function contour map of orbital $8a_g$ (LUMO) in the xy plane.

Discussion

Two of the most striking features of the d^2 imido complexes described here are their structural diversity [pseudotetrahedral (e.g., **5**), trigonal bipyramidal (**7**), and octahedral (**2**, **8**, **11**) geometries] and their relatively high reactivity. While it is difficult to predict, a priori, the structure of d^n complexes containing π-bonded ligands, there are several unifying principles that interrelate the complexes described here.

In the qualitative MO description for ML_4 complexes in T_d symmetry, the ligand σ-type orbitals transform as $A_1 + T_2$ and interact with the metal s, p_x, p_y, and p_z most strongly to form the a_1 and t_2 σ orbitals.[14] The d_{xy}, d_{yz}, and d_{xz} (T_2) also participate in σ-bonding in a three-orbital mixing interaction and so become weakly antibonding in T_d. The $d_{x^2-y^2}$ and d_{z^2} orbitals (E) are essentially nonbonding. The π bonds in a tetrahedral ML_4 complex transform as $E + T_1 + T_2$, and $E + T_2$ sets are of the correct symmetry to interact with all five d orbitals, leaving three ligand-centered nonbonding orbitals of T_1 symmetry. Therefore, a complex that contains five π bonds will have no remaining metal-centered nonbonding orbitals. When the number of potential π bonds that can be formed with the ligand set is less than the number of d orbitals that are available, the LUMO is a metal-centered non- or weakly antibonding orbital. For a ligand set with a sufficient number of orbitals and electrons to form five π bonds the LUMO is either a σ- or a π-type antibonding orbital depending on the relative strengths of the σ and π interactions. This can be generalized as follows: d^n complexes with a ligand set with a capacity to form m π bonds will be stable in T_d geometry for all ($n/2 + m \leq 5$) configurations, since no antibonding orbitals are filled. However, $Os(NAr)_2(PMe_2Ph)_2$ is d^4 with the capacity to form four π bonds. Therefore, $n/2 + m = 6$; i.e., the "extra" electron pair would have to be placed in a σ- or π-antibonding orbital. This is the reason that **4b** adopts a trans square-planar geometry in which only three of the four potential π bonds can form, four electrons can be localized in osmium-centered nonbonding orbitals, and two electrons can be localized in the ligand-based nonbonding orbital.

The four-coordinate alkyl complexes (**10** and **14**) almost certainly are pseudotetrahedral, since each complex is d^2, four π bonds can be formed, and therefore $n/2 + m = 5$. If the complex had a trans square-planar geometry, the electron count in metal-based orbitals would be only 16. While this fact alone does not rule out their being trans square planar, a recent crystal structure of d^2 $W(NAr)_2(PMePh_2)_2$ (isoelectronic with **10** and **14**) shows it to be pseudotetrahedral,[15] consistent with the crystal structure of pseudotetrahedral d^2 $W(NAr)_2(PMe_2Ph)(\eta^2\text{-}OCMe_2)$[1v] and with

(15) Williams, D. S.; Davis, W. M. Unpublished results.

the argument that an "18-electron" count and consequently pseudotetrahedral geometry are preferred.

The fact that the metallaimidazolidine ring is planar in **5a** requires some comment. For a tetrahedral complex of type **5** in C_{2v} symmetry, the π bonds to the two terminal ligands transform as $A_2 + B_1$ (out-of-plane) + $A_1 + B_2$ (in-plane). These linear combinations of p orbitals interact with the metal d_{xy}, d_{xz}, ($d_{x^2-y^2}/d_{z^2}$), and d_{yz} orbitals, respectively. The nitrogen p orbitals in the ring transform as $A_2 + B_1$. Because these orbitals cannot interact with any additional metal d orbitals, the total number of π bonds remains at 4. Therefore two electrons can remain in a metal-centered nonbonding (d) orbital, and the resulting complex becomes an 18-electron species. That is not to say that the ring nitrogen p orbitals do not also participate in π bonding, as they could share the a_2 and b_1 molecular orbitals, with the largest coefficients most likely being found on the imido nitrogen atoms.

To our knowledge, no structures of octahedral bis(imido) d^2 complexes (e.g., **2**, **8**, and **11**) have been determined. They should be analogous to structurally characterized octahedral d^2 complexes that contain two trans oxo ligands. Examples include $[MoO_2(CN)_4]^{4-}$ and $[ReO_2(CN)_4]^{3-}$ (O–M–O = 180°),[16] $[ReO_2(en)_2]^+$ (O–M–O = 179.3 (3)°),[17] and $[OsO_2(en)_2]^+$ (O–M–O = 180°).[18] In an octahedral complex, all metal p orbitals are involved in σ-bonding. Therefore, the linear combination of p orbitals on the oxo ligands which could form π bonds to the metal remain essentially nonbonding. Of the three metal-centered orbitals that could form π bonds (d_{xy}, d_{xz}, and d_{yz}), only two can form π bonds to trans ligands. The third (d_{xy}) remains nonbonding.

The proposal that d^n complexes in which m π bonds can form will adopt tetrahedral structures only if $n/2 + m \leq 5$ is consistent with several known structures. For example, d^2 complexes of the type $M(NR_2)_4$ ($m = 4$) are tetrahedral.[19] In Mo(S-*t*-Bu)$_4$[20] and W(S-*t*-Bu)$_4$,[21] which are slightly "squashed" tetrahedra, the relatively small M–S–C angles suggest that sulfur can only form one π bond with the metal, i.e., $m = 4$. The almost linear W–O–C angles in W(O-2,6-$C_6H_3Me_2)_4$[22] and W(O-2,6-C_6H_3-*i*-$Pr_2)_4$,[22] on the other hand, suggest that $m = 8$, and both in fact are square planar. However, several known structures do not agree with predictions. For example, although the structure of Mo(O-*t*-Bu)$_4$[23] is not known, it is assumed to be tetrahedral because of its paramagnetism. Perhaps the *tert*-butoxide ligands can only form one π bond each to the metal ($m = 4$), not 2 π bonds ($m = 8$). Also, both $[RuO_4]^{2-}$ and $[FeO_4]^{2-}$ are tetrahedral, not square planar. Perhaps the oxygen p orbitals are energetically mismatched with the iron and ruthenium d orbitals, and therefore only weak π bonds can form, along with relatively low-lying π-antibonding orbitals, occupation of which is not especially destablizing. The correlation of H–E–H angles with electronegativity of the element E (O, S, Se) has been discussed in terms of a second-order Jahn–Teller distortion.[24] In a transition-metal complex, it is reasonable to expect that the same forces are at work, so how many π bonds can form unfortunately often will be difficult to assign unequivocally. For "invariant" π donors such as (terminal) nitrido (2π) and alkylidyne (2π) ligands, on the other hand, the above principles would seem to have greater applicability.

The observed trigonal-bipyramidal structure of **7** (presumably **9** and **15** have similar structures) is unusual because the two imido ligands are essentially linear (each imido ligand in has the capacity to form two π bonds to the metal) and the N–Os–N angle is large (151.2 (3)°). The large N–Os–N angle is consistent with anticipated steric effects, but it also can be explained on the basis of an electronic argument. Of crucial importance is the fact that there are metal-centered d orbitals of appropriate symmetry to engage in π bonding with all four combinations of nitrogen 2p orbitals (Scheme IV). Since 5 electron pairs are involved in σ bonding, a fairly ideal TBP could be regarded as a genuine "20-electron" species; i.e., 2 electrons must be localized in a π-antibonding orbital.

Scheme IV. Correlation Diagram for the Distortion of a TBP Species (e.g., **7**) to a Related Square-Pyramidal Species by Opening the N–Os–N Angle

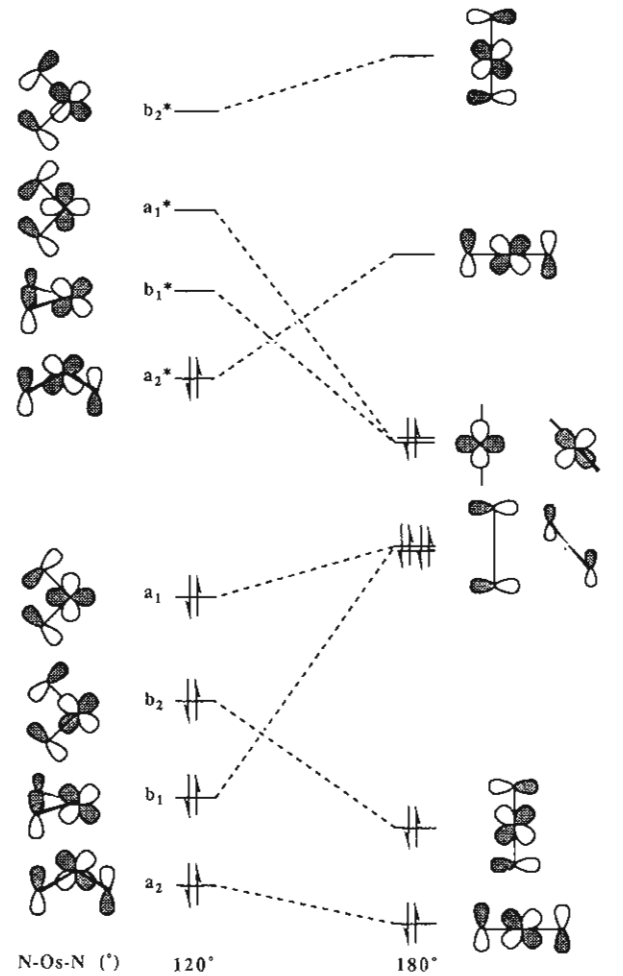

Now suppose that the N–Os–N angle is opened up to give a tetragonal species that contains an apical iodide (Scheme IV). Taking the π molecular orbitals perpendicular to the *yz* plane first, the a_2 molecular orbital forms a stronger π bond at 180° than at 120°. As a consequence, the antibonding combination is raised in energy. The b_1 combination behaves differently. As the N–Os–N angle is increased, the nitrogen p orbitals are no longer able to overlap with the osmium d orbital constructively. At the 180° limit the π and π^* molecular orbitals of b_1 symmetry are reduced to two nonbonding orbitals, one metal-centered and one ligand-centered. The in-plane π orbitals follow similar trends. One combination (b_2) forms a more stable π molecular orbital, while the other (a_1) degenerates into its metal- and ligand-centered components, which are fully nonbonding at the 180° limit. The important feature is that four electrons end up in a ligand-based nonbonding orbital and the complex can be formulated in this geometry as a "16-electron" species. The observed N–Os–N angle could be interpreted as resulting from a distortion away from 120° (in order to eliminate electron density in the π^* orbital) but not so much that the metal becomes electron deficient in the 180°

(16) Day, V. W.; Hoard, J. L. *J. Am. Chem. Soc.* **1968**, *90*, 3374.
(17) Lock, C. J. L.; Turner, G. *Acta Crystallogr.* **1978**, *B34*, 923.
(18) Malin, J. M.; Schlemper, E. O.; Murmann, R. K. *Inorg. Chem.* **1977**, *16*, 615.
(19) (a) Bradley, D. C.; Chisholm, M. H. *Acc. Chem. Res.* **1976**, *9*, 273. (b) Bradley, D. C.; Chisholm, M. H. *J. Chem. Soc. A* **1971**, 2741. (c) Chisholm, M. H.; Cotton, F. A.; Extine, M. W. *Inorg. Chem.* **1978**, *17*, 1329.
(20) Otsuka, S.; Kamata, M.; Hirotsu, K.; Higuchi, T. *J. Am. Chem. Soc.* **1981**, *103*, 3011.
(21) Listemann, M. L.; Dewan, J. C.; Schrock, R. R. *J. Am. Chem. Soc.* **1985**, *107*, 7207.
(22) Listemann, M. L.; Schrock, R. R.; Dewan, J. C.; Kolodziej, R. M. *Inorg. Chem.* **1988**, *27*, 264.
(23) Cayton, R. H.; Chisholm, M. H.; Clark, D. L.; Hammond, C. E. *J. Am. Chem. Soc.* **1989**, *111*, 2751.
(24) Albright, T. A.; Burdett, J. K.; Whangbo, M.-H. *Orbital Interactions in Chemistry*; Wiley: New York, 1985.

limit. The compromise is when N–Os–N ≈ 150°. X-ray studies of several pseudotetrahedral d^2 bis oxo complexes suggest that the O–M–O angle is opened to 135–145° for electronic reasons alone.[28]

The reactivity of four- and five-coordinate bis(imido) d^2 species reported must be a direct consequence of the fact that four-, five-, and six-coordinate species can all be formed relatively readily, perhaps in part because of the "flexible" characteristics of the imido ligand as a π-bonding ligand. Therefore, nucleophiles can add to a four- or five-coordinate complex or be lost from a five- or six-coordinate complex. For example, reactions such as **7** → **15** could proceed either via phosphine loss first to give $Os(NAr)_2I_2$ or by addition of a methyl group to give "$[Os(NAr)_2I_2LMe]^-$"; both intermediates are reasonable. In contrast, complexes such as $[Os(N)R_4]^-$ are comparatively robust and unreactive.[1q]

Future studies will be aimed at expanding the examples of bis(imido) d^2 complexes beyond osmium, rhenium, and tungsten and exploiting the reactivity of such species, we hope in catalytic reactions.

Experimental Section

General Procedures. All experiments were performed under a nitrogen atmosphere in a Vacuum Atmospheres HE43-2 drybox or by using standard Schlenk techniques. Reagent grade diethyl ether, dimethoxyethane, and tetrahydrofuran were distilled from sodium benzophenone ketyl under nitrogen. Reagent grade toluene was distilled from molten sodium under nitrogen. Commercial grade pentane was washed with 5% nitric acid in sulfuric acid, stored over calcium chloride, and distilled from sodium benzophenone ketyl under nitrogen. Reagent grade dichloromethane was distilled from calcium hydride prior to use. Pyridine was stirred over potassium hydroxide and distilled from calcium hydride under nitrogen. In general, deuterated NMR solvents were dried by passage through a column of activated alumina and stored over molecular sieves.

^1H and ^{13}C NMR data are listed in parts per million downfield from TMS. Coupling constants are quoted in hertz. Obvious multiplicities and routine coupling constants usually are not listed. ^{31}P NMR spectra are referenced to external $P(OMe)_3$ at 141.0 ppm, and ^{19}F NMR spectra are referenced to external CCl_3F at 0.0 ppm in the solvent of interest. Spectra were obtained at 25 °C unless otherwise noted. Elemental analyses were performed by Schwarzkopf Microanalytical Laboratory (Woodside, NY) or in our own laboratory with a Perkin-Elmer PE-2400 Microanalyzer.

SCF-Xα-SW Calculations. All calculations were carried out on either a Silicon Graphics or VAX workstation using a program based on the original Xα–SW code of Johnson and Smith.[3,4] A set of atomic coordinates (1 bohr = 0.529 177 Å) was first generated for each model in idealized geometry (D_{3h} for $Os(NH)_3$; C_{2h} for *trans*-$Os(NH)_2(PH_3)_2$). Sets of atomic sphere radii were calculated according to the Norman criterion,[25] and because the overlap for the core atoms (i.e. Os, N, P) was determined not to be excessive (<25%), they were used without further scaling. This was confirmed (in both cases) by a satisfactory virial ratio ($-2T/V \approx 1.000$) in the final calculation. Exchange correlation parameters (α values) were taken from Schwarz,[26] except for α_H where the value suggested by Slater[27] was used. The α value for the outer-sphere and interatomic regions were calculated as the weighted average of the α values for the constituent atoms, based on the number of valence electrons for each atom. The wave functions were expanded from partial waves (atomic angular momenta) on each atomic center where the l_{max} for each center was as follows: outer-sphere and interatomic region, 5; osmium, 3; nitrogen and phosphorus, 2; hydrogen, 1. A molecular potential was generated by the superposition of atomic potentials, and this potential was used for the spin-restricted calculation of an initial set of wave functions. The levels were populated according to Fermi statistics, and a new molecular potential was generated. A fraction of the new potential was mixed in with the old potential, and the resulting potential was used as the starting point for the next calculation. This eliminated dramatic fluctuations in the molecular potential as the model reached self-consistency.

Preparation of Compounds. $Os(NAr)_3$ (1). A mixture consisting of OsO_4 (2.0 g, 7.87 mmol) and 2,6-diisopropylphenyl isocyanate (4.8 g, 23.65 mmol) was refluxed in 35 mL of heptane under argon for 20 h. Upon cooling of the reaction mixture to ambient temperature, red-brown crystals were deposited from solution. These were isolated by filtration and dried in vacuo to yield (2.84 g, 50%) red-brown prisms: ^1H NMR (C_6D_6) δ 7.33 (t, H_p), 7.03 (d, H_m), 3.84 (sept, C*H*Me$_2$), 1.21 (d, CH*Me*$_2$); ^{13}C NMR (C_6D_6) δ 155.70 (C_{ipso}), 139.45 (C_o), 128.21 (C_p), 123.27 (C_m), 29.10 (*C*HMe$_2$), 22.93 (CH*Me*$_2$); mass spectrum (EI) *m/e* 717 ([M]$^+$, ^{192}Os, correct isotope distribution for $C_{36}H_{51}N_3Os$). Anal. Calcd for $C_{36}H_{51}N_3Os$: C, 60.39; H, 7.18; N, 5.87. Found: C, 60.60; H, 7.22; N, 5.77.

$Os(NAr)_2Cl_2(py)_2$ (2). A solution of pyHCl in 10 mL of CH_2Cl_2 (0.323 g, 2.8 mmol) was added to a solution of $Os(NAr)_3$ (1.0 g, 1.4 mmol) in 30 mL of CH_2Cl_2. The resulting mixture was stirred at 25 °C for 5 days. The product was dried in vacuo and the residue washed with pentane until the washings were colorless. The residue was then extracted into 50 mL of benzene, the extract was filtered, and the filtrate was evaporated to dryness to afford a brown powder. The product was recrystallized from a 1:1 mixture of benzene and pentane to yield 0.43 g (40%): ^1H NMR (C_6D_6) δ 9.20 (d, 4, py Hα), 7.04 (m, 6, Ar $H_{m/p}$), 6.63 (t, 2, py H_α), 6.28 (t, 4, py H_β), 3.83 (sept, 4, C*H*Me$_2$), 1.05 (d, 24, CH*Me*$_2$); $^{13}C\{^1H\}$ NMR (C_6D_6) δ 156.10 (py C_β), 151.33 (py C_β), 149.88 (Ar C_{ipso}), 138.19 (Ar C_o), 125.71 (Ar C_p), 124.62 (py C_γ), 123.49 (Ar C_m), 27.48 (*C*HMe$_2$), 24.69 (CH*Me*$_2$). Anal. Calcd for $C_{34}H_{44}Cl_2N_4Os$: C, 53.05; H, 5.76; N, 7.28. Found: C, 52.63; H, 5.77; N, 7.07.

$Os(NAr)_3O$ (3). A suspension of $Os(NAr)_3$ (0.2 g, 0.28 mmol) and Me_3NO (63 mg, 0.84 mmol) was stirred at ambient temperature for 12 h in toluene (15 mL). The solvents were removed in vacuo, and the residue was recrystallized from pentane (ca. 50 mL) to afford 0.15 g (73%) of red-brown crystals: ^1H NMR (C_6D_6) δ 7.00 (d, 6, Ar H_m), 6.88 (t, 3, Ar H_p), 3.47 (sept, 6, C*H*Me$_2$), 1.08 (d, 36, CH*Me*$_2$); $^{13}C\{^1H\}$ NMR (C_6D_6) δ 153.77 (Ar C_{ipso}), 141.33 (Ar C_o), 128.59 (Ar C_p), 122.51 (Ar C_m), 29.31 (*C*HMe$_2$), 23.55 (CH*Me*$_2$); IR (Nujol; cm^{-1}) 836 (s, ν(OsO)); mass spectrum (EI) *m/e* 733 ([M]$^+$ ^{192}Os, correct isotope distribution for $C_{36}H_{51}N_3OOs$). Anal. Calcd for $C_{36}H_{51}N_3OOs$: C, 59.07; H, 7.02; N, 5.74. Found: C, 58.75; H, 7.17; N, 5.65.

$Os(NAr)_2(PMe_3)_2$ (4a). Trimethylphosphine (0.43 mL, 4.2 mmol) was added to a suspension of $Os(NAr)_3$ (1.0 g 1.4 mmol) in 10 mL of pentane at −40 °C. After 2 h crystals began to form. The mixture was cooled to −40 °C, and 0.82 g (85%) of purple crystals were filtered off, washed with cold pentane (2 × 5 mL), and dried in vacuo: ^1H NMR (C_6D_6) δ 6.99–6.85 (m, 6, Ar $H_{m/p}$), 4.49 (sept, 4, C*H*Me$_2$), 1.30 (t, J = 5.5, 18, PMe_3), 1.29 (d, 24, CH*Me*$_2$); $^{13}C\{^1H\}$ NMR (C_6D_6) δ 153.90 (Ar C_{ipso}), 139.14 (Ar C_o), 122.55 (Ar C_m), 120.73 (Ar C_p), 27.13 (*C*HMe$_2$), 23.78 (CH*Me*$_2$), 17.60 (t, J = 29.3, PMe_3); $^{31}P\{^1H\}$ NMR (C_6D_6) δ −37.12; UV–vis (CH_2Cl_2; nm) 565 (ε = 27 000), 525 (sh, ε = 18 000). Anal. Calcd for $C_{30}H_{52}N_2OsP_2$: C, 52.00; H, 7.56; N, 4.04. Found: C, 52.21; H, 7.63; N, 3.87.

$Os(NAr)_2(PMe_2Ph)_2$ (4b). A solution of dimethylphenylphosphine (0.8 mL, 5.63 mmol) in 5 mL of pentane was added to a suspension of $Os(NAr)_3$ (1.343 g, 1.89 mmol) in 10 mL of pentane at −40 °C. After 12 h at room temperature the solution was cooled to −35 °C to afford 1.23 g (80%) of red-purple crystals, which were washed with cold pentane and dried in vacuo: ^1H NMR (C_6D_6) δ 8.03 (m, 4, H_o), 7.18–7.05 (m, 6, $H_{m/p}$), 6.93–6.84 (m, 6, $H_{m/p}$), 4.32 (sept, 4, C*H*Me$_2$), 1.53 (t, J = 5.4, 12, P*Me*$_2$Ph), 1.13 (d, 24, CH*Me*$_2$); $^{13}C\{^1H\}$ NMR (C_6D_6) δ 153.78 (C_{ipso}), 139.53 (C_o), 133.48, 129.64 ($C_{m,p}$), 122.53 (C_m), 120.93 (C_p), 27.53 (*C*HMe$_2$), 24.15 (CH*Me*$_2$), 16.50 (t, J = 28, P*Me*$_2$Ph); $^{31}P\{^1H\}$ NMR (C_6D_6) δ −24.66; UV/vis (CH_2Cl_2; nm) 571 (ε = 25 000). Anal. Calcd for $C_{32}H_{45}N_2OsP_2$: C, 58.80; H, 6.91; N, 3.43. Found: C, 58.62; H, 7.14; N, 3.45.

$Os(NAr)_2[P(OMe)_3]_2$ (4c). Trimethyl phosphite (0.25 mL, 2.1 mmol) was added to a suspension of $Os(NAr)_3$ (0.5 g, 0.70 mmol) in 10 mL of pentane. The blue-purple solution was stirred at room temperature for 24 h, and the solvent was removed in vacuo to afford an oily blue-purple solid. Repeated recrystallizations from pentane afforded 0.287 g (52%) of blue-purple crystals: ^1H NMR (C_6D_6) δ 7.0–6.8 (m, 6, $H_{m/p}$), 4.50 (sept, 4, C*H*Me$_2$), 3.49 (t, J = 11, 18, P(O*Me*)$_3$), 1.33 (d, 24, CH*Me*$_2$); $^{13}C\{^1H\}$ NMR (C_6D_6) δ 154.30 (C_{ipso}), 140.72 (C_o), 122.17 (C_m), 121.93 (C_p), 52.34 (P(O*Me*)$_3$), 27.65 (*C*HMe$_2$), 24.21 (CH*Me*$_2$); $^{31}P\{^1H\}$ NMR (C_6D_6) δ 107.34. Anal. Calcd for $C_{30}H_{52}N_2O_6OsP_2$: C, 45.68; H, 6.64; N, 3.55. Found: C, 45.69; H, 6.62; N, 3.54.

Os[(Ar)CH$_2$CH$_2$NAr](NAr)(O) (5a). A solution of $Os(NAr)_3O$ (0.5 g, 0.684 mmol) in 20 mL of toluene was cooled to −78 °C, and 1 atm of C_2H_4 was placed over the solution. After the solution was stirred under ethylene at 25 °C for 18 h, the solvents were removed in vacuo and the residue was recrystallized from pentane to afford 0.40 g (78%) of

(25) Norman, J. G. *Mol. Phys.* **1976**, *31*, 1191.
(26) (a) Schwarz, K. *Phys. Rev. B.: Solid State* **1972**, *5*, 2466. (b) Schwarz, K. *Theor. Chim. Acta* **1974**, *34*, 225.
(27) Slater, J. C. *Int. J. Quantum Chem.* **1973**, *S7*, 533–544.
(28) (a) Cai, S.; Hoffman, D. M.; Wierda, D. A. *Polyhedron* **1990**, *9*, 957. (b) Stavropoulos, P.; Edwards, P.; Behling, T.; Wilkinson, G.; Motevalli, M.; Hursthouse, M. B. *J. Chem. Soc., Dalton Trans.* **1987**, 169. (c) Longley, C. J.; Savage, P. D.; Wilkinson, G.; Hussain, B.; Hursthouse, M. B. *Polyhedron* **1988**, *7*, 1079. (d) Perrier, S.; Kochi, J. K. *Inorg. Chem.* **1988**, *27*, 4165.

red-black crystals: ^{1}H NMR (C_6D_6) δ 7.15–6.80 (m, 9, $H_{m/p}$), 4.05 (AA′BB′, 4, C_2H_4), 3.79 (sept, 2, C*H*Me$_2$), 2.81 (sept, 2, C*H*Me$_2$), 2.41 (sept, 2, C*H*Me$_2$), 1.54 (d, 6, CH*Me*$_2$), 1.20 (d, 6, CH*Me*$_2$), 1.14 (d, 6, CH*Me*$_2$), 0.92 (d, 6, CH*Me*$_2$), 0.89 (d, 12, CH*Me*$_2$); ^{13}C{^{1}H} NMR (C_6D_6) δ 154.00 (C_{ipso}), 152.50 (C_{ipso}), 147.17 (C_o), 144.28 (C_o), 138.51 (C_o), 128.18 ($C_{m/p}$), 125.97 ($C_{m/p}$), 125.59 ($C_{m/p}$), 124.46 ($C_{m/p}$), 121.76 ($C_{m/p}$), 70.21 (C_2H_4), 28.42 (*C*HMe$_2$), 28.40 (*C*HMe$_2$), 27.87 (*C*HMe$_2$), 26.06 (CH*Me*$_2$), 26.00 (CH*Me*$_2$), 23.07 (CH*Me*$_2$), 23.02 (CH*Me*$_2$), 22.97 (CH*Me*$_2$); IR (Nujol; cm^{-1}) 896 (s, ν(OsO)); mass spectrum (EI) *m/e* 761 ([M]$^+$, ^{192}Os). Anal. Calcd for $C_{38}H_{55}N_3OOs$: C, 60.05; H, 7.29; N, 5.53. Found: C, 60.18; H, 7.44; N, 5.70.

Os(ArNC$_7$H$_{10}$NAr)O(NAr) (5b). Os(NAr)$_3$O (0.2 g, 0.274 mmol) was treated with norbornene (51.5 mg, 0.54 mmol) at 25 °C in 15 mL of pentane for 18 h. The solution was concentrated to dryness, and the residue was recrystallized from pentane to afford 0.104 g (46%) red-brown crystals: ^{1}H NMR (C_6D_6) δ 7.12–6.80 (m, 9, $H_{m/p}$), 4.30 (s, 2, NBE C_α), 3.89 (sept, 2, C*H*Me$_2$), 2.92 (sept, 2, C*H*Me$_2$), 2.31 (s, 2, NBE C_β), 2.19 (sept, 2, C*H*Me$_2$), 1.66 (d, 6, CH*Me*$_2$), 1.36 (d, 6, CH*Me*$_2$), 1.22 (d, 6, CH*Me*$_2$), 1.15–1.00 (m, 4, NBE), 0.89 (d, 18, CH*Me*$_2$), 0.71–0.66 (m, 2, NBE); ^{13}C{^{1}H} NMR (C_6D_6) δ 154.45, 151.66, 147.09, 143.71, 138.52, 126.06, 125.73, 125.03, 121.51 (C_{Ar}), 89.82 (NBE C_α), 43.08 (NBE C_β), 32.53, 28.91, 28.43, 28.15, 27.02, 25.91, 25.25, 24.44, 23.64 (NBE, *C*HMe$_2$, CH*Me*$_2$); IR (Nujol; cm^{-1}) 892 (s, ν(OsO)); mass spectrum (EI) *m/e* 827 ([M]$^+$, ^{192}Os). Anal. Calcd for $C_{43}H_{61}N_3OOs$: C, 62.51; H, 7.44; 5.09. Found: C, 62.97; H, 7.65; N, 4.99.

Observation of Os(ArNC$_5$H$_8$NAr)O(NAr) (5c). Cyclopentene (1.1 g, 1.35 mmol) was added at room temperature to a sample of Os(NAr)$_3$O (25 mg, 0.031 mmol) in C_6D_6 in an NMR tube: ^{1}H NMR (C_6D_6) δ 7.15–6.79 (m, 9, $H_{m/p}$), 4.83 (m, 2, C_5H_8 H_α), 3.87 (sept, 2, C*H*Me$_2$), 2.92 (sept, 2, C*H*Me$_2$), 2.18 (sept, 2, C*H*Me$_2$), 2.1–1.95 (br m, 1, C_5H_γ), 1.62 (d, 6, C*H*Me$_2$), 1.6–1.5 (br m, 2, C_5H_8), 1.4 (br m, 1, C_5H_8), 1.31 (d, 6, CH*Me*$_2$), 1.21 (d, 6, CH*Me*$_2$), 0.90 (d, 6, CH*Me*$_2$), 0.88 (d, 6, CH*Me*$_2$).

Os(NAr)$_2$O$_2$ (6). Os(NAr)$_2$(PMe$_2$Ph)$_2$ (0.7 g, 0.86 mmol) was treated with trimethylamine oxide (0.26 g, 3.43 mmol) in 20 mL of CH_2Cl_2 at 25 °C for 24 h. Within 30 min the initial blue color had turned orange-brown. After 24 h the solvents were removed in vacuo and the residue was extracted into pentane (30 mL). The extract was filtered and concentrated in vacuo, and the crystals of the OPMe$_2$Ph byproduct were removed. The remaining solid was recrystallized from pentane at −35 °C to afford 0.22 g (45%) of red-brown crystals: ^{1}H NMR (C_6D_6) δ 6.92–6.84 (m, 6, $H_{m/p}$), 3.40 (sept, 4, *C*HMe$_2$), 1.07 (d, 24, CH*Me*$_2$); ^{13}C{^{1}H} NMR (C_6D_6) δ 152.36 (C_{ipso}), 144.56 (C_o), 131.18 (C_p), 122.91 (C_m), 28.90 (*C*HMe$_2$), 22.99 (CH*Me*$_2$); IR (Nujol; cm^{-1}) 883 (s, ν_{sym}(OsO$_2$)), 877 (s, ν_{asym}(OsO$_2$)). Anal. Calcd for $C_{24}H_{34}N_2O_2Os$: C, 50.38, H, 5.98, N, 4.89. Found: C, 50.61; H, 6.27; N, 5.01.

Os(NAr)$_2$I$_2$(PMe$_2$Ph) (7). A mixture of Os(NAr)$_2$(PMe$_2$Ph)$_2$ (1.1 g, 1.35 mmol) and I_2 (0.34 g, 1.35 mmol) in 30 mL of toluene at 25 °C was left standing for 16 h. The solvents were removed in vacuo to afford a deep blue residue. The product was extracted into toluene (10 mL), and methyl iodide (0.38 g, 2.7 mmol) was added. The volatile components were removed in vacuo, and the residue was recrystallized from benzene/pentane (1:5) to afford 1.01 g (80%) of blue crystals: ^{1}H NMR (CD_2Cl_2) δ 7.4–7.1 (m, 11, C_{Ar}), 3.07 (sept, 4, C*H*Me$_2$), 1.94 (d, 6, P*Me*$_2$Ph), 1.18 (br m, 24, CH*Me*$_2$); ^{31}P{^{1}H} NMR (CD_2Cl_2) δ −25.36; UV–vis (toluene; nm) 632 (ϵ = 26 300). Anal. Calcd for $C_{32}H_{48}I_2N_2OsP$: C, 41.21; H, 4.86; N, 3.00. Found: C, 41.45; H, 4.89; N, 2.84.

Os(NAr)$_2$I$_2$(PMe$_3$)$_2$ (8). The preparation of **8** was similar to that of **7** from Os(NAr)$_2$I$_2$(PMe$_2$Ph) (0.3 g, 0.215 mmol) and PMe$_3$ (2.15 mmol, 222 μL) in 25 mL of dichloromethane. The product was recrystallized from a mixture of dichloromethane and pentane (1:10) at −40 °C to afford 0.1 g (50%) of blue microcrystals: ^{1}H NMR ($CDCl_3$) δ 7.2–7.0 (m, 6, aryl), 3.10 (br s, 4, C*H*Me$_2$), 1.65 (t, 18, J = 8.5, P*Me*$_3$), 1.22 (br, 24, $\Delta_{1/2}$ = 40, CH*Me*$_2$); ^{13}C{^{1}H} NMR ($CDCl_3$) δ 134.7 (br, C_o), 129.6 (br, C_p), 123.6 (br, C_m), 29.3 (br, *C*HMe$_2$), 28.0 (br, *C*HMe$_2$), 25.5 (br, CH*Me*$_2$), 24.0 (CH*Me*$_2$), 14.4 (t, J = 54, PMe$_3$); ^{31}P{^{1}H} NMR ($CDCl_3$) δ −17.74; UV–vis (CH_2Cl_2; nm) 231 (ϵ = 57 000), 280 (ϵ = 45 000), 634 (ϵ = 24 500).

Os(NAr)$_2$MeI(PMe$_2$Ph) (9a). Methyl iodide (48.8 μL, 0.78 mmol) was added to a solution of Os(NAr)$_2$(PMe$_2$Ph)$_2$ (0.32 g, 0.39 mmol) in 30 mL of toluene at 25 °C. After 16 h, the mixture was concentrated to dryness, and the residue was recrystallized first from benzene/pentane and then from toluene/pentane to afford 0.31 g (95%) blue-purple crystals: ^{1}H NMR (C_6D_6) δ 7.9–6.9 (m, 11, $H_{o/m/p}$), 3.63 (d, J = 3.3, 3, Os–C*H*$_3$), 3.51 (sept, 2, C*H*Me$_2$), 2.70 (sept, 2, C*H*Me$_2$), 1.84 (d, J = 11, 6, P*Me*$_2$Ph), 1.39 (d, 6, CH*Me*$_2$), 1.25 (d, 6, CH*Me*$_2$), 1.14 (d, 6, CH*Me*$_2$), 1.13 (d, 6, CH*Me*$_2$); ^{13}C{^{1}H} NMR (C_6D_6) δ 154.51 (C_{ipso}), 142.09 (C_o), 139.87 (C_o′), 132.13 (d, J = 60, P–C_{ipso}), 130.14 (d, J = 11, P–C_o), 129.11 (d, J = 11, P–C_m), 125.18 (C_p), 123.62 (C_m), 122.79 (C_m′), 29.51 (*C*HMe$_2$), 29.09 (*C*HMe$_2$), 26.64 (CH*Me*$_2$), 25.20 (CH*Me*$_2$), 23.62 (CH*Me*$_2$), 21.40 (CH*Me*$_2$), 13.86 (d, J = 41, P*Me*$_2$Ph), −15.10 (Os–*C*H$_3$); ^{31}P{^{1}H} NMR (C_6D_6) δ −25.33; UV–vis (toluene; nm) 599 (ϵ = 71 000). Anal. Calcd for $C_{33}H_{48}IN_2OsP$: C, 48.29; H, 5.89; N, 3.41. Found: C, 47.96; H, 5.76; N, 3.11.

Os(NAr)$_2$EtI(PMe$_2$Ph) (9b). A solution (15 mL of toluene) containing Os(NAr)$_2$(PMe$_2$Ph)$_2$ (0.1 g, 0.123 mmol) and EtI (9.9 μL, 0.123 mmol) was stirred for 12 h. Methyl iodide (7.7 μL, 0.123 mmol) was added and the mixture stirred for a further 30 min at room temperature. The mixture was concentrated to dryness, and the residue was recrystallized from a mixture of benzene and pentane at −40 °C to afford 0.071 g (70%) of deep blue crystals: ^{1}H NMR (C_6D_6) δ 7.4–6.7 (m, 11, aryl), 4.18 (qd, J = 7.4 and 4.4, 2, CH_2CH_3), 3.78 (sept, 2, C*H*Me$_2$), 3.02 (sept, 2, C*H*Me$_2$), 2.17 (t, J = 7.2, 3, CH_2CH_3), 1.65 (d, 6, CH*Me*$_2$), 1.38 (d, 6, CH*Me*$_2$), 1.26 (d, 6, CH*Me*$_2$), 1.18 (d, J = 11, 6, P*Me*$_2$Ph), 1.12 (d, 6, CH*Me*$_2$); ^{13}C{^{1}H} NMR (C_6D_6) δ 154.85 (C_{ipso}), 142.90 (C_o), 139.98 (C_o′), 131.51 (d, J = 63.7, P–C_{ipso}3o), 130.79 (d, J = 9.8, P–$C_{o/m}$), 130.11 (d, J = 8.3, P–$C_{o/m}$), 129.35 (P–C_p), 125.02 (C_p), 124.02 (C_m), 122.80 (C_m′), 29.76 (CH_2CH_3), 29.16 (*C*HMe$_2$), 28.67 (*C*HMe$_2$), 27.11 (CH*Me*$_2$), 25.61 (CH*Me*$_2$), 23.55 (CH*Me*$_2$), 21.48 (CH*Me*$_2$), 13.00 (d, J = 37.2, P*Me*$_2$Ph), 5.37 (CH_2CH_3); ^{31}P{^{1}H} NMR (C_6D_6) −31.35.

[Os(NAr)$_2$Me(PMe$_2$Ph)][PF$_6$] (10). To a solid mixture of Os(NAr)$_2$MeI(PMe$_2$Ph) (0.36 g, 0.439 mmol) and AgPF$_6$ (0.111 g, 0.439 mmol) was added 20 mL of cold (−40 °C) dichloromethane. The mixture was stirred in the dark for 3 h, during which time the blue solution turned red-brown. The solution was concentrated to dryness, and the residue was recrystallized from a mixture of dichloromethane and pentane at −40 °C to afford 0.293 g (80%) of red microcrystals: ^{1}H NMR (CD_2Cl_2) δ 7.51 (t, 2, H_p), 7.5–7.3 (m, 5, P–aryl), 7.21 (d, 4, H_m), 3.88 (s, 3, Os–C*H*$_3$), 3.09 (sept, 4, C*H*Me$_2$), 2.30 (d, J = 13, 6, P*Me*$_2$Ph), 1.26 (d, 12, CH*Me*$_2$), 1.18 (d, 12, CH*Me*$_2$); ^{13}C{^{1}H} NMR (CD_2Cl_2) δ 146.62 (C_{ipso}), 133.60 (C_o), 130.86 (C_p), 130.22 (P–$C_{o/m}$), 129.94 (P–C_{ipso}), 129.72 (P–$C_{o/m}$), 30.18 (*C*HMe$_2$), 23.95 (CH*Me*$_2$), 22.98 (CH*Me*$_2$), 17.84 (d, J = 44, P*Me*$_2$Ph), −14.31 (q, J = 138, Os–*C*H$_3$); ^{31}P{^{1}H} NMR (CD_2Cl_2) δ −11.72 (PMe$_2$Ph), −144.35 (sept, J = 710, PF_6); ^{19}F NMR (CD_2Cl_2) δ 33.45 (d, J = 710, PF_6). Anal. Calcd for $C_{33}H_{48}F_6N_2OsP_2$: C, 47.25; H, 5.77; N, 3.34. Found: C, 47.42; H, 5.74; N, 3.35.

Os(NAr)$_2$(S$_2$CNEt$_2$)$_2$ (11). THF (10 mL cooled to −40 °C) was added to a stirred solid mixture of Os(NAr)$_2$I$_2$(PMe$_2$Ph) (0.3 g, 0.32 mmol) and potassium diethyldithiocarbamate (0.12 g, 0.64 mmol). After 16 h the mixture was concentrated to dryness and the resulting residue was recrystallized from a mixture of toluene and pentane (1:3) at −35 °C to afford 0.19 g (71%) of deep blue crystals: ^{1}H NMR (C_6D_6) δ 7.07 (d, 4, H_m), 6.85 (t, 2, H_p), 4.69 (sept, 4, C*H*Me$_2$), 2.99 (q, J = 7.2, 8, CH_2CH_3), 1.52 (d, 24, CH*Me*$_2$), 0.63 (t, J = 7.2, 12, CH_2CH_3); ^{13}C{^{1}H} NMR (C_6D_6) δ 220.94 (S_2CNEt_2), 150.96 (C_{ipso}), 148.99 (C_o), 123.95 (C_p), 122.84 (C_m), 44.47 (CH_2CH_3), 29.10 (*C*HMe$_2$), 25.50 (CH*Me*$_2$), 12.02 (CH_2CH_3); mass spectrum (EI) *m/e* 838 ([M]$^+$, ^{192}Os); UV–vis (toluene; nm) 611 (ϵ = 46 800), 572 (sh, ϵ = 36 200). Anal. Calcd for $C_{30}H_{44}N_4OsS_4$: C, 48.77; H, 6.50; N, 6.69. Found: C, 48.96; H, 6.28; N, 6.43.

Os(NAr)$_2$(O$_2$CMe)$_2$(PMe$_2$Ph) (12). A mixture of Os(NAr)$_2$I$_2$(PMe$_2$Ph) (1.22 g, 1.31 mmol) and AgOAc (0.46 g, 2.73 mmol) in 30 mL of dichloromethane was stirred at ambient temperature in the dark for 20 h. The mixture was filtered, and the filtrate was concentrated to dryness. The residue was recrystallized from a mixture of dichloromethane and pentane at −40 °C to afford 0.99 g (95%) of blue needles: ^{1}H NMR (CD_2Cl_2) δ 7.86 (ddd, 2, Ph H_o), 7.38–7.58 (m, 3, Ph $H_{m/p}$), 7.0–7.1 (m, 6, $H_{m/p}$), 3.78 (sept, 4, C*H*Me$_2$), 2.14 (d, J = 12, 6, P*Me*$_2$Ph), 1.96 (s, 6, OCO*CH*$_3$), 1.08 (d, 24, CH*Me*$_2$); ^{13}C{^{1}H} NMR (CD_2Cl_2) δ 184.58 (O*C*OCH$_3$), 152.32 (C_{ipso}), 147.95 (C_o), 133.13 (d, J = 65, Ph C_{ipso}), 132.11 (d, J = 9.3, Ph C_o), 131.66 (Ph C_p), 128.76 (d, J = 13, C_m), 126.14 (C_p), 123.12 (C_m), 24.27 (*C*HMe$_2$), 22.87 (OCO*C*H$_3$), 20.26 (CH*Me*$_2$), 17.66 (d, J = 43, P*Me*$_2$Ph); ^{31}P{^{1}H} NMR (CD_2Cl_2) δ −23.66; UV–vis (CH_2Cl_2; nm) 663 (ϵ = 18 500).

Os(NAr)$_2$(S-*t*-Bu)$_2$ (13). A solution of Os(NAr)$_2$(OAc)$_2$(PMe$_2$Ph) (0.05 g, 0.063 mmol) and LiS-*t*-Bu (12 mg, 0.13 mmol) in 10 mL of toluene was stirred at ambient temperature for ~3 h, during which time the color changed from deep blue to red-brown. The volatile components were removed in vacuo, and the residue was extracted with 20 mL of pentane. The extract was filtered through Florisil, and the filtrate was concentrated and cooled to −40 °C to afford 45 mg (70%) of blood red crystals: ^{1}H NMR (C_6D_6) δ 7.28 (2, H_p), 6.96 (4, H_m), 3.98 (4, C*H*Me$_2$), 1.48 (18, SC*Me*$_3$), 1.31 (24, CH*Me*$_2$); ^{13}C{^{1}H} NMR (C_6D_6) δ 154.46 (C_{ipso}), 146.21 (C_o), 128.96 (C_p), 124.15 (C_m), 50.05 (*C*Me$_3$), 33.50 (SC*Me*$_3$), 27.98 (*C*HMe$_2$), 23.82 (CH*Me*$_2$). Anal. Calcd for $C_{32}H_{52}N_2OsS_2$: C, 53.45; H, 7.29; N, 3.90. Found: C, 53.47; H, 7.07; N, 3.78.

Os(NAr)$_2$(CH$_2$CMe$_3$)$_2$ (14a). A cold (−40 °C) solution of Me$_3$CCH$_2$MgCl (0.170 mL, 1.48 M, 0.252 mmol) in 6 mL of diethyl

ether was added to a cold (−40 °C) solution of $Os(NAr)_2(OAc)_2(PMe_2Ph)$ (0.1 g, 0.126 mmol) in 10 mL of ether. At room temperature a red-brown solution formed immediately. After 2 h the mixture was filtered through Celite and the solvents were removed in vacuo. The residue was suspended in 10 mL of cold pentane and treated with *n*-PrOH (~0.5 mL) for ~20 s. The residue was purified further by flash chromatography on basic alumina, eluting with pentane. The orange solution was concentrated in vacuo and cooled to −40 °C to afford 46 mg (53%) of orange crystals: ^1H NMR (C_6D_6) δ 7.24 (t, 2, H_p), 6.99 (d, 4, H_m), 4.43 (s, 4, CH_2CMe_3), 3.77 (sept, 4, $CHMe_2$), 1.30 (d, 24, $CHMe_2$), 1.14 (s, 18, CH_2CMe_3); $^{13}C\{^1H\}$ NMR (C_6D_6) δ 154.37 (C_{ipso}), 145.08 (C_o), 126.69 (C_p), 123.31 (C_m), 37.68 (CH_2CMe_3), 32.60 (CH_2CMe_3), 29.07 ($CHMe_2$), 23.87 ($CHMe_2$), 23.78 (t, CH_2CMe_3). UV-vis (pentane; nm) 579 (ϵ = 395); mass spectrum (EI) *m/e* 684 ($[M]^+$, ^{192}Os). Anal. Calcd for $C_{34}H_{56}N_2Os$: C, 59.79; H, 8.26; N, 4.10. Found: C, 59.86; H, 8.35; N, 3.96.

$Os(NAr)_2(CH_2SiMe_3)_2$ (14b). A cold (−40 °C) solution of Me_3SiCH_2MgCl (0.64 mL, 1.41 M, 0.904 mmol) in diethyl ether was added to a stirred suspension of $Os(NAr)_2(OAc)_2(PMe_2Ph)$ (0.36 g, 0.452 mmol) in 10 mL of diethyl ether at −40 °C. Upon being warmed to room temperature, the solution turned orange-brown. After 3 h the mixture was taken to dryness and the residue was extracted with 30 mL of pentane. The extract was filtered through Celite and purified further by flash chromatography through basic alumina to give an orange solution, which was concentrated and cooled to −40 °C to afford 0.217 g (67%) of orange-red crystals: ^1H NMR (C_6D_6) δ 7.23 (t, 2, H_p), 6.96 (d, 4, H_m), 3.80 (s, 4, CH_2SiMe_3), 3.62 (sept, 4, $CHMe_2$), 1.27 (d, 24, $CHMe_2$), 0.13 (s, 18, CH_2SiMe_3); $^{13}C\{^1H\}$ NMR (C_6D_6) δ 154.64 (C_{ipso}), 144.95 (C_o), 128.07 (C_p), 123.21 (C_m), 28.77 ($CHMe_2$), 23.25 ($CHMe_2$), 1.02 (CH_2SiMe_3), −14.99 (CH_2SiMe_3); UV-vis (pentane; nm) 640 (ϵ = 476). Anal. Calcd for $C_{32}H_{56}N_2OsSi_2$: C, 53.74; H, 7.89; N, 3.92. Found: C, 53.91; H, 7.74; N, 3.94.

$Os(NAr)_2Me_2(PMe_2Ph)$ (15). A cold (−40 °C) solution of MeMgBr (0.325 mL, 3.3 M in diethyl ether, 1.07 mmol) in 8 mL of diethyl ether was added to a cooled suspension of $Os(NAr)_2I_2(PMe_2Ph)$ in 20 mL of ether (0.5 g, 0.54 mmol). The mixture was stirred at room temperature for 20 h and filtered through Celite. The solvent was removed from the filtrate in vacuo, and the residue was recrystallized from pentane to afford 0.31 g (82%) blue crystals: ^1H NMR (CD_2Cl_2, −40 °C) δ 7.3–6.8 (m, 11, aryl), 3.44 (sept, 2, $CHMe_2$), 3.25 (d, J = 6.3, 3, Os–CH_3), 2.78 (sept, 2, $CHMe_2$), 1.60 (d, J = 7.8, 3, Os–CH_3), 1.55 (d, J = 6.6, 6, PMe_2Ph), 1.22 (d, J = 6.6, 6, $CHMe_2$), 1.14 (d, 6, $CHMe_2$), 1.12 (d, 6, $CHMe_2$), 0.95 (d, 6, $CHMe_2$); $^{31}P\{^1H\}$ NMR (CD_2Cl_2) δ −38.04; UV-vis (pentane; nm) 605 (ϵ = 13 200). Anal. Calcd for $C_{34}H_{51}N_2OsP$: C, 57.60; H, 7.25; N, 3.95. Found: C, 57.46; H, 7.14; N, 4.27.

Structure of $Os(NAr)[N(Ar)CH_2CH_2N(Ar)]O$ (5a). Data were collected at 23 °C on an Enraf-Nonius CAD-4 diffractometer with graphite-monochromated Mo Kα radiation (λ = 0.710 69 Å). Of the 9205 reflections that were collected, 8507 were unique, equivalent reflections were merged. The intensities of three representative reflections measured after every 60 min of X-ray exposure time remained constant throughout data collection. (No decay correction was applied.) The structure was solved by the Patterson method and refined by full-matrix least squares by using TEXSAN. The non-hydrogen atoms were refined anisotropically. Hydrogens were included in calculated positions (d_{C-H} = 0.95 Å). Crystal data may be found in Table II.

Structure of $Os(NAr)_2I_2(PMe_2Ph)$ (7). Data were collected at 23 °C on an Rigaku AFC6R diffractometer with graphite-monochromated Mo Kα radiation (λ = 0.710 69 Å) and a 12-kW rotating anode generator. Of the 8504 reflections that were collected, 8029 were unique. The intensities of three representative reflections measured after every 60 min of X-ray exposure time remained constant throughout data collection (No decay correction was applied.) An empirical absorption correction, based on azimuthal scans of several refections, was applied, which resulted in transmission factors ranging from 0.75 to 1.00. The structure was solved by direct methods and refined by full-matrix least squares by using TEXSAN. The non-hydrogen atoms were refined anisotropically. Hydrogens were included in calculated positions (d_{C-H} = 0.95 Å). Crystal data may be found in Table II.

Acknowledgment. R.R.S. thanks the National Science Foundation for research support (Grant 88-22508) and the U.S. Department of Energy, Division of University and Industry Programs, for funds to purchase the X-ray diffractometer (Grant DE-FG05-86ER75292). J.T.A. thanks the Deutscher Akademischer Austauschdienst for a NATO Postdoctoral Fellowship, and T.P.K. thanks the Science and Engineering Research Council for a NATO Postdoctoral Fellowship.

Supplementary Material Available: For $Os(NH)_3$ in D_{3h} symmetry and $Os(NH)_2(PH_3)_2$ in C_{2h} symmetry tables of Xα parameters and for **5a** and **7** labeled ORTEP drawings and tables of final positional parameters, final thermal parameters, bond distances and angles, and torsion angles (40 pages); tables of final observed and calculated structure factors (112 pages). Ordering information is given on any current masthead page.